SARS-CoV-2 infection models using *in vivo* and *in vitro* hACE2-lentivirus transduction

Daniel J. Rawle[1*], Thuy Le[1], Troy Dumenil[1], Kexin Yan[1], Bing Tang[1], Cameron Bishop[1], Andreas Suhrbier[1,2].

[1] Immunology Department, QIMR Berghofer Medical Research Institute, Brisbane, Queensland. 4029, Australia.
[2] GVN Center of Excellence, Australian Infectious Disease Research Centre, Brisbane, Queensland 4029 and 4072, Australia.

[*]Corresponding author. Email: Daniel.Rawle@qimrberghofer.edu.au

SUMMARY

SARS-CoV-2 uses the human ACE2 receptor (hACE2), with mouse ACE2 (mACE2) unable to support infection. Herein we describe an ACE2-lentivirus system and illustrate its utility *in vitro* and *in vivo*. Transduction of non-permissive cell lines with hACE2 imparted replication competence, and transduction with mACE2 containing N30D, N31K, F83Y and H353K mutations, to match hACE2, rescued SARS-CoV-2 replication. hACE2-lentivirus transduction of C57BL/6J, IFNAR$^{-/-}$ and IL-28RA$^{-/-}$ mice lungs indicated type I and III IFN receptor knockout had minimal effect on virus replication. However, RNA-Seq illustrated that they were required for inflammatory responses in C57BL/6J mice, which were similar to those seen in COVID-19 patients. Finally, we illustrate the utility of hACE2 transduction for vaccine evaluation in C57BL/6J mice. The hACE2-lentivirus system thus has broad application in SARS-CoV-2 research, in particular allowing access to GM mice, while also offering the inherent advantages of lentiviral transduction such as stable genomic integration.

KEYWORDS

SARS-CoV-2, lentivirus, ACE2, GM mice, vaccination, mutations, interferon, inflammation, RNA-seq

INTRODUCTION

Severe acute respiratory syndrome coronavirus 2 (SARS-CoV-2) has spread rapidly into a global pandemic (Wu et al., 2020a). SARS-CoV-2 infection can be asymptomatic, but is also the etiological agent of coronavirus disease 2019 (COVID-19), with acute respiratory distress syndrome (ARDS) representing a common severe disease manifestation (Guan et al., 2020). The SARS-CoV-2 pandemic has sparked unprecedented global research to understanding mechanisms of virus replication and disease pathogenesis, and to generate vaccines and treatments. Key to these efforts has been the development of animal models of SARS-CoV-2 infection and COVID-19 disease (Muñoz-Fontela et al., 2020).

The receptor binding domain (RBD) of the spike glycoprotein of SARS-CoV-2 binds human Angiotensin-Converting Enzyme 2 (hACE2) as the primary receptor for cell attachment and entry (Zhao et al., 2020). Mice do not support productive virus replication because the SARS-CoV-2 spike binds poorly to mouse ACE2 (mACE2) (Zhou et al., 2020). Expression of hACE2 in mice often via a transgene allows SARS-CoV-2 infection and can recapitulate aspects of COVID-19, with hACE2 expressed under control of various promoters, including K18 (Golden et al., 2020; McCray et al., 2007; Moreau et al., 2020; Oladunni et al., 2020; Rathnasinghe et al., 2020; Winkler et al., 2020; Yinda et al., 2021), mACE2 (Bao et al., 2020; Sun et al., 2020b), HFH4 (Jiang et al., 2020b), or chicken β-actin (Tseng et al., 2007). These mouse models all differ in various aspects including level of virus replication, disease manifestations and tissue tropisms (Muñoz-Fontela et al., 2020), but do not provide a simple mechanism whereby genetically modified (GM) mice can be exploited for SARS-CoV-2/COVID-19 research. Two systems that do allow the latter, involve transient hACE2 expression in mouse lungs using adenovirus vectors (Ad5) or adeno-associated virus (AAV), which impart the capacity for productive SARS-CoV-2 replication in mouse lungs (Hassan et al., 2020; Israelow et al., 2020; Rathnasinghe et al., 2020). A third involves use of mouse adapted SARS-CoV-2 (Dinnon et al., 2020; Gu et al., 2020; Leist et al., 2020), although use of this mutated virus may complicate evaluation of interventions targeting human SARS-CoV-2.

Lentivirus-mediated gene expression in mice lung epithelium has been investigated as a treatment for cystic fibrosis and provides long term expression of the cystic fibrosis transmembrane conductance regulator (CFTR) (Alton et al., 2017b; Buckley et al., 2008; Copreni et al., 2010; Copreni et al., 2004; Kremer et al., 2007; Limberis et al., 2010; Wilson, 2004). These studies demonstrated that VSV-G pseudotyped lentivirus can transduce mouse airway epithelial cells and their progenitors resulting in long-term gene expression. Herein we describe an ACE2-lentiviral system that conveys SARS-CoV-2 replication competence *in vitro* and allows productive infection of mouse lungs *in vivo*. We illustrate that GM mice can thereby be accessed for SARS-CoV-2/COVID-19 research, with experiments using IFNAR$^{-/-}$ and IL-28RA$^{-/-}$ mice showing the importance of type I and III IFN responses for SARS-CoV-2-induced inflammation. We also illustrate the use of hACE2-lentiviral transduction of lungs of wild-type C57BL/6J mice for evaluation of vaccines.

RESULTS

hACE2-lentiviruses for evaluating the role of RBD binding residues

hACE2 coding sequence (optimized for mouse codon usage) was cloned into the dual promoter lentiviral vector pCDH-EF1α-MCS-BGH-PGK-GFP-T2A-Puro (herein referred to as pCDH) (Figure 1A), which had been modified to contain the full length EF1α promoter. Previous studies show the EF1α promoter effectively drives gene expression after intranasal VSV-G pseudotyped lentivirus transduction of mouse lungs (Alton et al., 2017a). The GFP marker and puromycin resistance gene (cleaved from GFP by T2A) is expressed from a separate 3-phosphoglycerate kinase (PGK) promoter (Fig 1A). VSV-G pseudotyped pCDH-hACE2 lentivirus was produced by co-transfection of the lentiviral vector with VSV-G and Gag-Pol-Rev plasmids in HEK293T cells, and was used to transduce HEK293T (human embryonic kidney)

cells followed by puromycin selection. HEK293T cells do not express hACE2 (Crawford et al., 2020) and therefore do not support SARS-CoV-2 replication, whereas HEK293T cells transduced with hACE2 supported substantial virus replication (Figure 1A). A T92Q mutation in hACE2 was introduced to determine if removing the N90 glycosylation motif increased SARS-CoV-2 replication, as computer-based modelling predicted enhanced affinity for spike RBD with removal of this glycan (Chan et al., 2020; Mehdipour and Hummer, 2020). We also introduced K31N/K353H and T27Y/L79Y/N330Y mutations into hACE2 as these changes were predicted by computer modeling to reduce and enhance affinity for spike RBD (Chan et al., 2020), respectively. HEK293T cells expressing these aforementioned hACE2 mutations did not significantly affect SARS-CoV-2 replication (Fig 1B), suggesting that the N90 glycan, and K31/K353 residues in hACE2 are not alone key determinants of viral infectivity.

Characterizing residues responsible for the inability of mACE2 to support SARS-CoV-2 replication

The ACE2-lentivirus system was used to introduce amino acid substitutions into mACE2 to identify amino acids that make mACE2-expressing cells unable to support SARS-CoV-2 replications. Analysis of crystal structures and species susceptibilities has suggested residues that may be responsible for the differences in binding of the RBD to hACE2 and mACE2 (Alexander et al., 2020; Damas et al., 2020; Griffin et al., 2020; Rodrigues et al., 2020; Wang et al., 2020). Based on these *in silico* studies, we identified seven residues potentially responsible for the human-mouse differences. mACE2-lentivirus vectors were then generated that contained all seven substitutions (N30D/N31K/T79L/S82M/F83Y/A329E/H353K), with two further vectors constructed to identify the minimum requirements for SARS-CoV-2 replication. The latter contained a subset of the seven changes; four amino acid changes (N30D/N31K/F83Y/H353K) and two amino acid changes (N31K/H353K).

As expected HEK293T cells expressing mACE2 did not support productive SARS-CoV-2 replication, and CPE was not observed. In contrast, all three mACE2 mutants rescued virus replication and infection resulted in CPE (Figure 1C-D). However, virus replication was ≈1 log lower for cells expressing mACE2 with only two substitution (N31K/H353K) (Figure 1C) and infection produced less CPE (Figure 1D). Thus two amino acid changes (N31K and H353K) in mACE2 were sufficient to support SARS-CoV-2 replication; however, at least four changes (N30D/N31K/F83Y/H353K) were required for virus replication and CPE to be comparable to that seen in cells expressing hACE2.

Thus of all the potential interactions between the RBD and ACE2 previously identify by X ray crystallography and of all the amino acid differences between human and mouse ACE2 (Damas et al., 2020; Wang et al., 2020), it emerges 4 are key to determining infectivity differences for cells expressing hACE2 or mACE2. In the aforementioned crystal structures, hACE2-D30 interacts with S-K417 via a salt bridge, hACE2-K31 interacts with S-Q493, hACE2-Y83 interacts with S-N487, and hACE2-K353 forms hydrogen bonds with S-G496 and S-G502 (Figure 1E). Our studies highlight the utility of the ACE2-lentivirus system for studying the role of ACE2 residues in productive SARS-CoV-2 infections.

hACE2-lentivirus transduction of mouse cell lines imparts SARS-CoV-2 replication competence

To determine whether hACE2-lentivirus transduction could make mouse cell lines SARS-CoV-2 replication competent and thus available for SARS-CoV-2 research, 3T3 (mouse embryonic fibroblasts) and AE17 (mouse lung mesothelioma cell line) cells were transduced with hACE2. Significant virus replication was seen in transduced cells (Supplementary Figure 1), although somewhat lower than that seen in transduced HEK293 cells. Overt CPE was not seen (Supplementary Figure 1). This illustrates that the hACE2-lentivirus system can be used for mouse cell lines, but that the efficiency of viral replication may be cell line or cell type dependent.

SARS-CoV-2 replication in hACE2-lentivirus transduced C57BL/6J, IFNAR$^{-/-}$ and IL-28RA$^{-/-}$ mice

lung

To illustrate the utility of the hACE2-lentivirus system for use in GM mice, we investigated the role of type I and type III IFN receptor signaling in controlling SARS-CoV-2 replication. C57BL/6J, IFNAR$^{-/-}$ and IL-28RA$^{-/-}$ were inoculated i.n. with 1.2-2.2×10^4 transduction units of hACE2-lentivirus, equivalent to approximately 190-350 ng of p24 per mice (Figure 2A). An hour prior to administration of lentivirus, mice were treated with 1% lysophosphatidylcholine (LPC) to enhance transduction efficiency (Kremer et al., 2007; Limberis et al., 2002). One week later mice were challenged with SARS-CoV-2 (10^5 $CCID_{50}$ i.n. per mice), and lungs were collected at 2, 4 and 6 days post infection (Fig 2A). Mice did not display overt clinical symptoms or weight loss (Figure 1B), consistent with some studies using Ad5-hACE2 (Rathnasinghe et al., 2020), but not others (Sun et al., 2020a). RT-qPCR analyses indicated similar levels of hACE2 mRNA after transduction of mouse lungs in each of the 3 mouse strains, with expression maintained over the 6 day course of the experiment (Figure 2C).

Lungs from infected C57BL/6J, IFNAR$^{-/-}$ and IL-28RA$^{-/-}$ were analysed for infectious virus tissue titers. Untransduced lungs showed no virus titers (Figure 2D), whereas hACE2-lentivirus transduced lungs showed significant viral titers ranging from 10^2 to 10^5 CCID50/g for all strains of mice on day 2, with titers dropping thereafter (Figure 2D). Viral RNA levels were measured using RT-qPCR, with untransduced lungs showing low and progressively decaying levels post-inoculation (Figure 2E). For all hACE2-lentivirus transduced lungs, significantly elevated and persistent viral RNA levels were seen for all strains and at all time points by RT-qPCR (Figure 2E). Reducing viral titers and lingering viral RNA have been reported previously for K18-hACE2 mice (Winkler et al., 2020) and is suggested in human infections (Jefferson et al., 2020). RNA-Seq also illustrated that virus replication in hACE2-lentivirus transduced lungs, K18-hACE2 transgenic mice and Ad5-hACE2 transduced lungs (Sun et al., 2020a) were comparable when normalized to hACE2 mRNA expression (Figure 2F), suggesting comparable hACE2 translation efficiencies in these different expression systems.

Importantly, no significant differences in viral loads emerged between C57BL/6J, IFNAR$^{-/-}$ and IL-28RA$^{-/-}$ mice (Figure 2D, E). This remained true even when viral RNA levels were normalized to hACE2 mRNA levels (Supplementary Figure 2). Similar results were obtained by RNA-Seq, with viral read counts not significantly different for the 3 mouse strains (Supplementary Figure 3A-D). Thus using three different techniques, no significant effects on viral replication could be seen in mice with type I or type III IFN receptor deficiencies.

SARS-CoV-2 replication in hACE2-lentivirus transduced mice lung induces interferon and cytokine signatures by day 2 post-infection

To determine the innate response to SARS-CoV-2 replication in hACE2-transduced mouse lungs, gene expression in lungs of infected hACE2-transduced mice was compared with that of inoculated untransduced mice at day 2 post-infection using RNA-Seq. Differentially expressed genes (DEGs) between these groups were identified using a false discovery rate (FDR, or q value) threshold of <0.05 (Figure 3A; Supplementary Table 1A-C). Of the 110 DEGs, 95 were upregulated, with ≈40% of these classified as type I IFN-stimulated genes (ISGs) as determined using Interferome (using conservative settings that only include genes validated *in vivo* for mice) (Figure 3B, full list in Supplementary Table 1D). Type III ISGs are poorly annotated in this database, and so this analysis likely under-estimates the number of these genes.

Ingenuity Pathway Analysis (IPA) of the 110 DEGs produced a series of pro-inflammatory Upstream Regulators (USRs) (Supplementary Table 1E-F) and included Th1, Th2 and Th17-associated cytokine USRs, as well as type I IFN USRs (Figure 3C). SARS-CoV-2-specific T cells in humans were reported to be predominantly Th1-assocaiated, but Th2-associated cytokines were also produced (Weiskopf et al., 2020). A cytokine and type I IFN DEG list has been published for a RNA-Seq analysis

of SARS-CoV-2 infected K18-hACE2 transgenic mice (Winkler et al., 2020). These DEG lists were used to interrogate the full pre-ranked (fold change) gene list (Figure 3A, Supplementary Table 1B) by Gene Set Enrichment Analysis (GSEA). Significant enrichments were observed (Figure 3D), indicating similar cytokine and interferon (IFN) responses after SARS-CoV-2 infection of K18-hACE2 transgenic and hACE2-lentivirus transduced mice.

IPA *Diseases and Functions* analysis of the 110 DEGs revealed a series of annotations dominated by cellular infiltration and innate responses signatures (Figure 3E, Supplementary Table G-H). Several of the annotations were associated with macrophages (Figure 3E), consistent with a previous report showing that inflammatory monocyte-macrophages (IMMs) were the major source of inflammatory cytokines in mouse adapted SARS-CoV infected mice (Channappanavar et al., 2016). Innate immune signaling was also the dominant signature in other analyses including GO Biological Processes and Cytoscape (Supplementary Table 1I-J).

GSEA analysis using the >31,000 gene signatures available from the molecular signatures database (MSigDB), indicated significant negative enrichment (negative NES scores) of gene sets associated with translation and mitochondrial electron transport chain function (Supplementary Table 1K). Translation inhibition by SARS-CoV-2 Nsp1 blocking mRNA access to ribosomes has been reported previously (Banerjee et al., 2020; Schubert et al., 2020). SARS-CoV-2 down-regulation of genes associated with cellular respiration and mitochondrial function has also been reported previously (Miller et al., 2021).

DEGs from human COVID-19 lung (Blanco-Melo et al., 2020) were also enriched in our hACE2-lentivirus transduced mouse lungs, and analysis of the core enriched genes indicated the similarity was due to cytokine, IFN, chemokine and inflammatory signaling genes (Figure 3F, Supplementary Table 1L-M). A different human COVID-19 lung dataset was also used (Wu et al., 2020b) and confirmed enrichment of immune-related DEGs in the hACE2-lentivirus transduced mice (Supplementary Table 1N). Overall this indicates that SARS-CoV-2 infection in hACE2-lentivirus transduced mice lungs recapitulates responses seen in other murine models and in COVID-19 patients.

Day 6 post-infection is characterized by inflammation resolution and tissue repair signatures

To determine how response profiles progress in the hACE2-lentivirus model, RNA-Seq was used to compare lungs on day 2 with lungs on day 6 post-infection, with day 6 broadly representing the time of severe lung disease in the K18-hACE2 model (Winkler et al., 2020). As noted above (Figure 2D), the virus titers had dropped in hACE2-lentivirus transduced mice lung over this time period by ≈2.8 logs, and severe disease (typically measured by weight loss) was not evident in this hACE2-lentivirus model (Figure 2B). In both hACE2-lentivirus transduced and untransduced C57BL/6J mice there was a clear evolution of responses from day 2 to day 6 post-infection; however, DEGs obtained from the former were largely distinct from DEGs obtained from the latter (Figure 4A). The RNA-Seq data thus illustrated that the DEGs associated with virus infection were distinct from those associated with virus inoculation (Figure 4A). RNA-Seq of infected lungs provided 551 DEGs, 401 up-regulated and 150 down-regulated (Figure 4B, Supplementary Table 2A-C).

IPA USR analyses of the 551 DEGs showed a clear reduction in inflammatory cytokine annotations, although the IL4 signature remained a dominant feature on day 6 (Figure 4C, Supplementary Table 2D-E). A Th2 skew and IL-4 have both been associated with lung damage in COVID-19 patients (Vaz de Paula et al., 2020). At day 6 there was an up-regulation of USRs primarily associated with tissue repair (Figure 4D, Supplementary Table 2F); MAPK1 (also known as ERK) and MAPK9 (Lavoie et al., 2020), BMP (Sountoulidis et al., 2012), TCF7L2 (Zhu et al., 2015), and KLF4 (Lin et al., 2017; Raslan and Yoon, 2020). B and T cell-associated USRs were also seen (Figure 4D, green circles) (Duperray et al., 1990; Nechanitzky et al., 2013; Wang et al., 2010), consistent with development of an adaptive

immune response. A relatively minor PARP1 signature was identified (Figure 4D), with PARP inhibitors being considered for COVID-19 therapy (Badawy, 2020; Curtin et al., 2020). A strong signature associated with estrogen receptor 1 (ESR1) was observed (Figure 4D), with estrogen having anti-inflammatory properties and believed to be associated with reduced COVID-19 severity in women (Jin et al., 2020; Peckham et al., 2020; Pinna, 2021), and reduced SARS-CoV disease severity in female mice (Channappanavar et al., 2016; Channappanavar et al., 2017). Follicle stimulating hormone (FSH) (Figure 4D) stimulates estrogen production, and inhibin subunit alpha (INHA) is involved in the negative feedback of FSH production (Nicks et al., 2010). IPA Diseases and Functions, Cytoscape, and GO Biological Processes analyses further supported the contention that on day 6 inflammation has abated and tissue repair is underway (Supplementary Table 2G-L).

The >31,000 gene sets available in MSigDB were used to interrogate the complete gene list (pre-ranked by fold change) for day 6 vs day 2 (Supplementary Table 2B) by GSEA. A highly significant negative enrichment for inflammatory response, and a highly significant positive enrichment for cilium development was seen (Figure 4E). Cilia in mammals are found in the lining of the respiratory epithelium. These GSEAs thus provide further support for the conclusion above, together arguing that in the hACE2-lentivirus model, day 6 post infection is characterized by inflammation resolution and tissue repair.

Type I and III IFN signaling is required for SARS-CoV-2-induced lung inflammation

To determine what responses to SARS-CoV-2 infection are dependent on type I IFN signaling, the lentivirus system was used to analyze IFNAR$^{-/-}$ mice lung using RNA-Seq. IFNAR$^{-/-}$ and C57BL/6J mice were transduced with hACE2-lentivirus and were then infected with SARS-CoV-2 and lungs harvested for RNA-Seq on days 2 and 6 post-infection. The largest impact of type I IFN signaling deficiency was seen on day 2 post infection (Figure 5A), consistent with disease resolution on day 6 (Fig 4C-E). The total number of DEGs for IFNAR$^{-/-}$ vs C57BL/6J mouse lungs on day 2 was 192, with most of these down-regulated (Figure 5A, Supplementary Table 3A-C). Viral reads were not significantly different between these two mouse strains (Figure 5A), confirming that knocking out type I IFN signaling is insufficient to affect SARS-CoV-2 replication (Frieman et al., 2010).

We showed in Figure 3 that RNA-Seq analysis revealed 110 DEGs associated with inflammatory responses when hACE2-transduced vs untransduced C57BL/6J mouse lungs on day 2 post infection were compared. When the same comparison was made for hACE2-lentivirus transduced vs untransduced lungs in SARS-CoV-2 infected IFNAR$^{-/-}$ mice, only 1 DEG (Kcnk5) was identified (Figure 5B). This clearly illustrated that the inflammatory responses on day 2 in C57BL/6J mice (Figure 3C) required intact type I IFN signaling.

As a control, the number of DEGs for IFNAR$^{-/-}$ mice vs C57BL/6J in untransduced lungs was determined. Although virus replication (hACE2-lentivirus transduced lung) provided 192 DEGs, virus inoculation (untransduced lung) provided only 16 DEGs (Figure 5C). Thus again, virus inoculation had a limited effect on these analyses, with DEGs largely arising from virus infection.

It is suggested that type III IFN acts as a first-line defense against infection at epithelial barriers, reserving the more potent and inflammatory type I IFN response in the event the type III IFN response is breached (Galani et al., 2017; Lazear et al., 2019). As type III IFN signaling has been implicated in reducing SARS-CoV-2 infection *in vitro* (Vanderheiden et al., 2020), the aforementioned analyses on day 2 was repeated in IL-28RA$^{-/-}$ mice. Viral reads were not significantly different between these two mouse strains (Figure 5D), confirming that knocking out type III IFN signaling was insufficient to affect SARS-CoV-2 replication (Boudewijns et al., 2020; Frieman et al., 2010). The DEG list for IL-28RA$^{-/-}$ vs C57BL/6J mice comprised 132 genes (Supplementary Table 4A-C), of which 84 were down-regulated (Figure 5D). Perhaps surprisingly, the DEG list was largely different from that seen in IFNAR$^{-/-}$ mice

(Figure 5D), arguing that the ISGs stimulated by these two pathways are distinct.

The majority (90%) of the 178 down-regulated DEGs in IFNAR$^{-/-}$ versus C57BL/6J mice at day 2 were ISGs according to the Interferome database (using *in vivo* and mouse only options) (Figure 5E, top and Supplementary Table 3D). Of the 84 down-regulated genes in IL-28RA$^{-/-}$ lungs, only 27% were identified as ISGs (Figure 5E, bottom and Supplementary Table 4D). However, there are no annotations in the Interferome database for type III ISGs in mice, and changing the settings to include human data (which is also under-annotated for type III IFN) did not increase the number of type III ISGs in our search using down DEGs from IL-28RA$^{-/-}$ lungs.

To determine the pathways regulated by type I and III IFN in response to SARS-CoV-2 infection, IPA USR analyses was performed on DEG lists from day 2 for hACE2-lentivirus transduced lungs for IFNAR$^{-/-}$ vs C57BL/6J (192 DEGs) and IL-28RA$^{-/-}$ vs C57BL/6J (132 DEGs). IPA USR signatures associated with pro-inflammatory cytokine signaling were significantly reduced in both IFNAR$^{-/-}$ and, to a lesser extent, IL-28RA$^{-/-}$ mice when compared to C57BL/6J mice (Figure 5F, full lists in Supplementary Table 3E and 4E). The same USR signatures (Figure 5F) were regulated by a largely distinct set of DEGs (Figure 5D), possibly due to differences in signaling kinetics and cell-type responsiveness to type I vs type III IFN (Lazear et al., 2019). Thus although there were not significant effects on viral replication, lungs from type I and type III IFN receptor knockout mice both had a blunted pro-inflammatory response to SARS-CoV-2 infection.

Immunization with infectious or UV-inactivated SARS-CoV-2 protects against virus infection

To evaluate the utility of the hACE2-lentivirus mouse model of SARS-CoV-2 replication for vaccination studies, mice were immunized subcutaneously (s.c.) twice with either infectious or UV-inactivated SARS-CoV-2 (Takasuka et al., 2004) formulated with adjuvant (Figure 6A). Serum SARS-CoV-2 neutralization titers were determined 4-9 weeks post-boost, and revealed all mice had serum neutralization titers (Figure 6B), comparable with high end levels seen in serum samples from prior SARS-CoV-2 infected individuals (Wajnberg et al., 2020). After challenge all mice were sacrificed on day 2 and all mice had detectable hACE2 mRNA, with hACE2 levels higher in unvaccinated mice (Figure 6C), perhaps due to cell infiltrates (see below) diluting hACE2 RNA levels. Mice vaccinated with both infectious and UV-inactivated SARS-CoV-2 showed significant reductions in viral RNA levels by RT-qPCR (Figure 6D), in tissue titrations (Figure 6E), and in RNA-Seq read counts (Figure 6F). These immunizations thus protected mice against significant viral infections and demonstrated the utility of hACE2-lentivirus transduced mice as a model for vaccine evaluation.

On day 2 the lungs were harvested and analyzed by RNA-Seq (all genes in Supplementary Table 5B), with 1376 DEGs identified for infectious virus immunization vs unimmunized (DEGs in Supplementary Table 5C). The DEGs were analyzed by IPA using canonical pathways, USR, and diseases and functions all showing infiltration signatures, dominated by T cell annotations (Supplementary Table 5D-F). This was confirmed by GSEA of human blood transcription modules (Li et al., 2014) against the pre-ranked (by fold change) gene list for immunized vs unvaccinated mice (Supplementary Table 5G). This showed the expected enrichment of T cell and B annotations in vaccinated mice (Figure 6F), and illustrated that protection against virus replication in lungs of immunized mice was associated with a significant infiltration of lymphocytes.

DISCUSSION

Here we describe a hACE2-lentivirus transduction system that allows the use of C57BL/6J and GM mice for SARS-CoV-2/COVID-19 research. Virus titer in hACE2-lentivirus transduced mice lung were comparable to other studies using mice transduced with Ad5 or AAV expressing hACE2 (Hassan et al.,

2020; Israelow et al., 2020; Rathnasinghe et al., 2020). These transduction methodologies have the advantage of avoiding the brain infection seen in K18-hACE2 mice, where brain infection is the major contributor to mortality (Carossino et al., 2021; Kumari et al., 2020). The key advantage of using lentiviral over adenoviral systems is integration of the lentiviral payload into the host cell genome, thus allowing long term stable expression. The development of the hACE2-lentivirus model of SARS-CoV-2 infection thus provides a new option which can be easily applied in laboratories with established lentiviral vector systems. We provide a detailed characterization of the lentivirus-hACE2 model of SARS-CoV-2 infection in C57BL/6J mice and illustrate the use of this model to evaluate the role of type I and type III IFNs in virus control and inflammation signatures, using IFNAR$^{-/-}$ and IL-28RA$^{-/-}$ mice. We also illustrate the use of C57BL/6J mice transduced with lentivirus-hACE2 for SARS-CoV-2 vaccine evaluation.

The lentivirus-hACE2 C57BL/6J mouse model of SARS-CoV-2 infection shares many cytokine signatures with those seen in human COVID-19 patients; IL-2, IL-10, IL-6, TNFα, IL-4, IL-1β, IFNγ and CSF3 signatures were found in SARS-CoV2-infected lentivirus-hACE2 transduced C57BL/6J mice on day 2 post infection, and elevated levels of these cytokines are found in COVID-19 patients (Han et al., 2020; Huang et al., 2020). Several of these cytokines have been implicated as mediators of COVID-19; for instance, IL-6 (Herold et al., 2020; Masiá et al., 2020; Xia et al., 2020), IL-4 (Vaz de Paula et al., 2020), IL-10 (Lu et al., 2021) and IFNγ (Gadotti et al., 2020). On day 6 post infection the lentivirus-hACE2 C57BL/6J mouse model showed a series of signatures associated with tissue repair. Thus our RNA-Seq analyses validate that this is a model of SARS-CoV-2 infection with acute inflammation and subsequent resolution.

We used the hACE2-lentivirus model of SARS-CoV-2 infection in IFNAR$^{-/-}$ and IL-28RA$^{-/-}$ mice to show that type I and III IFN signaling was involved in orchestrating the inflammatory response, while virus replication was not altered. This is largely in line with other studies using different model systems, which indicate that knocking out all IFN signaling (STAT1$^{-/-}$, STAT2$^{-/-}$, or combined IFNAR$^{-/-}$/IL-28RA$^{-/-}$ mice or hamsters) is required for increased virus replication (Boudewijns et al., 2020; Frieman et al., 2010; Israelow et al., 2020; Mahlakõiv et al., 2012). This suggests that having either type I or III IFN signaling alone is enough for partial restriction of virus replication in these mouse models. This is supported by *in vitro* experiments that show SARS-CoV-2 is sensitive to type I and III IFN, although infection doesn't stimulate particularly high levels of IFN (Felgenhauer et al., 2020; Vanderheiden et al., 2020), with SARS-CoV-2 encoding proteins that inhibit IFN signaling including Orf9b (Jiang et al., 2020a), Orf6 (Miorin et al., 2020), nsp6 and nsp13 (Xia et al., 2020). Thus while SARS-CoV-2 may be susceptible to IFN, the role of type I and III IFN signaling in driving inflammation has implications for proposed IFN therapies for COVID-19 patients (Monk et al., 2020).

Herein we also illustrate the use of the hACE2-lentivirus system to study the role of ACE2 residues on SARS-CoV-2 replication *in vitro*. We show that while the N31K and H353K substitutions in mACE2 increased SARS-CoV-2 replication compared to WT mACE2, the reverse mutation in hACE2 (K31N/K353H) did not affect virus replication compared to WT hACE2. This suggests that these residues alone are not true markers of species susceptibility or non-susceptibility, and the structure of the RBD binding region of ACE2 as a whole likely determines SARS-CoV-2 tropism. It also suggests that significant reductions in binding between spike RBD and ACE2 predicted *in silico* (Chan et al., 2020) do not always translate to reduced virus replication. This suggests that even low affinity interactions may be enough for productive virus replication, which has implications for design of hACE2 antagonists as antivirals. Our results may also inform a different approach to 'humanized' ACE2 mice where as few as two amino acid residues could be substituted in mACE2 to allow SARS-CoV-2 replication in mice.

In conclusion, we describe the development of a mouse model using intranasal hACE2-lentivirus transduction to sensitize mice lung to SARS-CoV-2 infection, which recapitulated cytokine signatures

seen in other mouse models and human COVID-19. We demonstrate broad applicability of this new mouse model in vaccine evaluation, GM mice infection, and *in vitro* evaluation of ACE2 mutants.

ACKNOWLEDGEMENTS

We thank Dr I Anraku for his assistance in managing the PC3 (BSL3) facility at QIMR Berghofer MRI. We thank Dr Alyssa Pyke and Mr Fredrick Moore (Queensland Health, Brisbane) for providing the SARS-CoV-2 isolate. We thank Dr. David Harrich for providing the lentivirus vectors. We thank Dr. Simon Phipps for providing the IL-28RA$^{-/-}$ mice. We thank Monash Genome Modification Platform for providing the plasmid containing the mouse-codon optimised human ACE2 gene. We thank Clive Berghofer and Lyn Brazil (and many others) for their generous philanthropic donations to support SARS-CoV-2 research at QIMR Berghofer MRI. A.S. holds an Investigator grant from the National Health and Medical Research Council (NHMRC) of Australia (APP1173880).

AUTHOR CONTRIBUTIONS

Conceptualization, D.J.R.; Methodology, D.J.R. and A.S.; Formal analysis, D.J.R., A.S., and T.D.; Investigation, D.J.R., T.L., K.Y., B.T.; Data curation, D.J.R., A.S., and T.D.; Writing – original draft, D.J.R.; Writing – review and editing, A.S. and D.J.R.; Visualization, D.J.R., A.S., T.D., and C.B; Supervision, D.J.R. and A.S., Project administration, D.J.R. and A.S.; Funding acquisition, A.S. and D.J.R.

DECLARATION OF INTERESTS

The authors declare no competing interests.

FIGURE LEGENDS

Figure 1. Mutational analyses of human and mouse ACE2 using ACE2-lentiviruses *in vitro*. A) Schematic of pCDH-EF1α-ACE2-BGH-PGK-GFP-T2A-Puro lentiviral vector. **B-C)** Growth kinetics of SARS-CoV-2 over a three day time course in HEK293T cells transduced with WT or mutant hACE2 **(B)** or mACE2 **(C)** infected at MOI=0.1. Data is the mean of 1 (mACE2-N31K/H353K) or 2 (all others) independent experiments with 3 replicates in each and error bars represent SEM. **D)** Inverted light microscopy images of HEK293T cells transduced with the indicated ACE2 lentivirus and infected with SARS-CoV-2 at MOI=0.1. Images were taken at 72 hpi and were representative of triplicate wells. **E)** Crystal structure of the Spike RBD:hACE2 complex (PBD: 6M0J) viewed in PyMOL and highlighting key interactions (blue) between hACE2 (red) and Spike RBD (green).

Figure 2. SARS-CoV-2 infection of mice lung after hACE2-lentivirus intranasal transduction. A) Timeline of lentivirus transduction of mice lung and SARS-CoV-2 infection. **B)** Percent weight loss for mice in C-E. **C)** RT-qPCR of mice lung RNA using primers for hACE2 (introduced by lentivirus transduction) normalized to mRPL13a levels. Data is individual mice and is expressed as RNA copy number calculated against a standard curve for each gene. Horizontal line indicates cut-off for reliable detection, with all untransduced mice falling below this line. **D)** Titer of SARS-CoV-2 in mice lung determined using $CCID_{50}$ assay of lung homogenate. Horizontal line indicates the limit of detection of 1.57 $\log_{10}$ CCID50/g. **E)** RT-qPCR of mice lung RNA using primers for SARS-CoV-2 E gene normalized to mRPL13a levels. Data is individual mice and is expressed as RNA copy number calculated using a standard curve. See Supplementary Figure 2 for SARS-CoV-2 RNA copies normalised to hACE2 copies. **F)** SARS-CoV-2 read counts (also see Supplementary Figure 3) normalized to hACE2 read counts from RNA-seq data for lentivirus-hACE2 transduced mice at day 2, K18-hACE2 transgenic mice at day 4, and Ad5-hACE2 transduced mice at day 2 (Sun et al., 2020a).

Figure 3. SARS-CoV-2 infection induces cytokine responses at 2 days post-infection in hACE2-lentivirus transduced mice. A) Volcano plot of gene expression from RNA-seq analyses of lung RNA at day 2 comparing mice with and without hACE2-lentivirus transduction. Genes were considered DEGs if they had a FDR value < 0.05 (above horizontal dotted line) (see Supplementary Table 1B-C for full gene and DEG lists). **B)** Interferome analysis of 95 up DEGs from 'A'. 38 of 95 up DEGs (40%) were ISGs. Red = type I IFN, blue = type II IFN, green = type III IFN (see Supplementary Table 1D for full Interferome ISG list). **C)** Cytokine signatures identified by IPA USR analysis (see Supplementary Table 1E-F for full and cytokine only USR lists) of 110 DEGs identified in 'A'. Circle area reflects the number of DEGs associated with each USR annotation. USRs were grouped into three categories; red = Th1 associated, green = Th2 associated, blue = Th17 associated, and black = pleiotropic/other. The vertical dotted line indicates activation z-score of 0. **D)** GSEAs for cytokine-related DEGs or type I IFN-related DEGs from Winkler et al. supplemental data (Winkler et al., 2020) against the pre-ranked all gene list (Supplementary Table 1B). Normalised enrichment score (NES) and nominal p-value are shown. **E)** IPA diseases and functions analysis (see Supplementary Table 1G-H for full lists) of 110 DEGs identified in 'A'. The 23 annotations with the most significant p-value and with an activation z-score of >2 were plotted with dots/lines indicating activation z-score and bars indicating $-\log_{10}$ p-value. Annotations were grouped into two categories; cellular infiltration (blue) and innate responses (red). **F)** GSEA for DEGs from human COVID-19 lung vs healthy control from Blanco-Melo et al. (Blanco-Melo et al., 2020) against the pre-ranked (by fold change) all gene list (Supplementary Table 1B). Normalised enrichment score (NES) and nominal p-value are shown. Core enriched genes (see Supplementary Table 1L for full core enriched gene list) determined by GSEA were entered into Enrichr and the top 10 GO Biological Processes annotations sorted by p-value are shown (see Supplementary Table 1M for full GO processes list).

Figure 4. Tissue repair signatures dominate at day 6 post-infection in hACE2-lentivirus transduced mice. A) Venn diagram for DEGs comparing day 6 vs 2 post infection with (red) and without (green) hACE2-lentivirus transduction. Number of DEGs that are FDR<0.05 are shown. Mean virus titer ($\log_{10}$ $CCID_{50}$/g) in lung tissue ± SEM (represents data shown in Figure 2D) is shown for hACE2 transduced mice at day 2 or 6 post infection. **B)** Volcano plot of gene expression from RNA-seq analyses of hACE2-lentivirus transduced lung RNA comparing day 6 with day 2 (see Supplementary Table 2B-C for gene and DEG lists). Genes were considered DEGs if they had a FDR value < 0.05 (above horizontal dotted line). **C)** Cytokine signatures identified by IPA USR analysis (see Supplementary Table 2D-E for full and cytokine only lists) of 551 DEGs identified in 'B' (Supplementary Table 2C). Circle area reflects the number of DEGs associated with each USR annotation. USRs were grouped into four categories; red = Th1 associated, green = Th2 associated, blue = Th17 associated, and black = pleiotropic/other. The vertical dotted line indicates activation z-score of 0. **D)** Upregulated USR signatures identified using IPA analysis (see Supplementary Table 2F) of 551 DEGs identified in 'B'. Circle area reflects the number of DEGs associated with each USR annotation. USRs (excluding chemicals) with an activation z-score of >2 are shown and were grouped into five categories; green = B cell function, blue = tissue repair – endocrine signaling, orange = tissue repair – growth factor, red = tissue repair – kinase, purple = tissue repair – Wnt signaling. **E)** Selected plots from GSEA of entire MSigDB database using pre-ranked (by fold change) 'all' gene list (Supplementary Table 2B). NES score and p-value is shown for the "GO_inflammatory_response" and "Wp_Genes_Related_To_Primary_Cilium_Development_Based_On_Crispr" annotations.

Figure 5. Type I and III IFN signaling is required for the cytokine response in C57BL/6J mice. A)

Venn diagram for number of DEGs (FDR<0.05) between IFNAR$^{-/-}$ vs C57BL/6J mice at day 2 or day 6 (green). Mean $\log_{10}$ SARS-CoV-2 read count in RNA-seq data ± SEM is shown (red text = day 2, green text = day 6). **B)** Venn diagram for number of DEGs (FDR<0.05) between plus vs minus hACE2-lentivirus transduction comparing C57BL/6J (red) and IFNAR$^{-/-}$ (green) mice at day 2. **C)** Venn diagram for IFNAR$^{-/-}$ vs C57BL/6J mice at day 2 comparing hACE2-lentivirus transduced (red) or untransduced (green) mice. **D)** Venn diagram comparing IFNAR$^{-/-}$ vs C57BL/6J (red) and IL-28RA$^{-/-}$ vs C57BL/6J (blue) (see Supplementary Table 3B-C and 4B-C for full gene and DEG lists) mice at day 2 (all mice had received hACE2-lentivirus transduction). Mean $\log_{10}$ SARS-CoV-2 read count in RNA-seq data ± SEM is shown (red text = IFNAR$^{-/-}$, black text = C57BL/6J, green text = IL-28RA$^{-/-}$). **E)** Interferome analysis of down DEGs from 'D'. See supplementary Table 3D and 4D for full Interferome ISG list. **F)** Signatures identified using IPA USR analysis of DEGs identified in 'D' for IFNAR$^{-/-}$ vs C57BL/6J (red) and IL-28RA$^{-/-}$ vs C57BL/6J (blue). Circle area reflects the number of DEGs associated with each USR annotation. Signatures were selected focusing on data previously identified in 'Figure 3C' (entire list is in Supplementary Table 3E and 4E).

Figure 6. Immunization protects against SARS-CoV-2 replication in hACE2-transduced mice lung and induces T and B cell responses. A) Timeline of mice vaccination, lentivirus transduction and SARS-CoV-2 infection. **B)** Reciprocal 50% neutralization titers of naïve mice and infectious or UV SARS-CoV-2 vaccinated mice. Horizontal dotted line represents the limit of detection (1 in 10). **C)** RT-qPCR of mice lung RNA using primers for hACE2 introduced by lentivirus transduction normalized to mRPL13a levels. Data is individual mice and is expressed as RNA copy number calculated against a standard curve for each gene. Horizontal line indicates cut-off for reliable detection, with all hACE2-negative mice falling below this line. **D)** RT-qPCR of mice lung RNA using primers for SARS-CoV-2 E gene normalized to mRPL13a levels. Data is individual mice and is expressed as RNA copy number calculated against a standard curve for each gene. **E)** Titer of SARS-CoV-2 in mice lung determined using $CCID_{50}$ assay of lung homogenate. Horizontal line indicates the limit of detection of 1.57 $\log_{10}$ CCID50/g. **F)** Mean $\log_{10}$ SARS-CoV-2 read count at day 2 post-infection in RNA-seq data ± SEM is shown (blue text = unvaccinated mice, red text = infectious SARS-CoV-2 immunized mice). GSEA for Blood Transcription Modules (BTMs) from Li et al. (Li et al., 2014) against the pre-ranked all gene list comparing unvaccinated vs infectious SARS-CoV-2 immunized (s.c) mice lung at day 2 (all mice had hACE2-lentivirus transduction). Selected BTM modules with a positive NES score and $p < 0.05$ are shown (full list in Supplementary Table 5). See Supplementary Table 5 for full gene and DEG lists and full downstream analyses lists.

STAR METHODS

Ethics statement

All mouse work was conducted in accordance with the "Australian code for the care and use of animals for scientific purposes" as defined by the National Health and Medical Research Council of Australia. Mouse work was approved by the QIMR Berghofer Medical Research Institute animal ethics committee (P3600, A2003-607). Mice were euthanized using CO_2 or cervical dislocation.

Cell lines and SARS-CoV-2 culture

Vero E6 (C1008, ECACC, Wiltshire, England; Sigma Aldridge, St. Louis, MO, USA), HEK293T, AE17, and NIH-3T3 cells were cultured in medium comprising RPMI1640 (Gibco) supplemented with 10% fetal calf serum (FCS), penicillin (100 IU/ml)/streptomycin (100 μg/ml) (Gibo/Life Technologies) and L-glutamine (2 mM) (Life Technologies). Cells were routinely checked for mycoplasma (MycoAlert Mycoplasma Detection Kit MycoAlert, Lonza) and FCS was assayed for endotoxin contamination before

purchase (Johnson et al., 2005). The SARS-CoV-2 isolate was kindly provided by Queensland Health Forensic & Scientific Services, Queensland Department of Health, Brisbane, Australia. The virus (hCoV-19/Australia/QLD02/2020) was isolated from a patient and sequence deposited at GISAID (https://www.gisaid.org/; after registration and login, sequence can be downloaded from https://www.epicov.org/epi3/frontend#1707af). Virus stock was generated by infection of Vero E6 cells at multiplicity of infection (MOI)≈0.01, with supernatant collected after 2-3 days, cell debris removed by centrifugation at 3000 x g for 15 min at 4°C, and virus aliquoted and stored at -80 °C. Virus titers were determined using standard $CCID_{50}$ assays (see below). The virus was determined to be mycoplasma free using co-culture with a non-permissive cell line (i.e. HeLa) and Hoechst staining as described (La Linn et al., 1995).

$CCID_{50}$ assays

Vero E6 cells were plated into 96 well flat bottom plates at $2x10^4$ cells per well in 100 µl of medium. For tissue titer, tissue was homogenized in tubes each containing 4 ceramic beads twice at 6000 x g for 15 seconds, followed by centrifugation twice at 21000 x g for 5 min before 5 fold serial dilutions in 100 µl RPMI1640 supplemented with 2% FCS. For cell culture supernatant, 10 fold serial dilutions were performed in 100 µl RPMI1640 supplemented with 2% FCS. 100 µl of serially diluted samples were added to Vero E6 cells and the plates cultured for 5 days at 37°C and 5% CO_2. The virus titer was determined by the method of Spearman and Karber (a convenient Excel $CCID_{50}$ calculator is available at https://www.klinikum.uni-heidelberg.de/zentrum-fuer-infektiologie/molecular-virology/welcome/downloads).

Lentivirus cloning

ACE2 genes were cloned into pCDH-EF1α-MCS-BGH-PGK-GFP-T2A-Puro Cloning and Expression Lentivector (System Biosciences, catalogue number CD550A-1), where the EF1α promoter was replaced with the full length EF1α using NheI and ClaI restriction enzymes (New England Biolabs). Human ACE2 coding sequence (codon optimized for mouse) was cloned into the pCDH lentivector using using PCR fragments amplified using Q5® High-Fidelity 2X Master Mix (New England Biolabs) and the following primers; vector backbone (pCDH amplified with Forward 5'- TAAATCGGATCCGCGG -3' and Reverse 5'- AATTCGAATTCGCTAGC) and hACE2 insert (Forward 5'- GCTAGCGAATTCGAATTATGAGCAGCAGCTCTTGGC -3' and Reverse 5'- CCGCGGATCGCATTTATCAGAAGCTTGTCTGCACGT -3'). The pCDH fragment was digested with DpnI (New England Biolabs) and was purified using QIAquick Gel Extraction Kit (QIAGEN), as was the hACE2 fragment. Fragments were recombined using NEBuilder HiFi DNA Assembly Cloning Kit as per manufacturer instructions. This was transformed into NEB® 10-beta Competent E. coli (High Efficiency) (New England Biolabs) as per manufacturer instructions and plated on ampicillin agar plates overnight. Colony PCR was performed using Q5 High-Fidelity 2X Master Mix (New England Biolabs) with the hACE2 insert primers to identify a positive colony, which was grown in LB broth with ampicillin and plasmid was purified using NucleoBond Xtra Midi kit (Machery Nagel).

All ACE2 mutant coding sequences were ordered from Twist Bioscience/Decode Science containing EcoRI upstream and BamHI downstream. Fragments were amplified using the using Q5® High-Fidelity 2X Master Mix (New England Biolabs) and the following primers; Forward 5'- CCTGACCTTAGCGAATTCATG -3' and Reverse 5'- ACCTAGCCTCGCGGATC -3'. PCR fragments were purified using Monarch DNA Gel Extraction Kit (New England Biolabs), and were digested with EcoRI and BamHI (New England Biolabs), as was the pCDH vector before purification again with Monarch® DNA Gel Extraction Kit (New England Biolabs). The ACE2 fragment was ligated with pCDH vector using T4 DNA Ligase (New England Biolabs) as per manufacturer instructions and then

transformed into NEB® 10-beta Competent E. coli (High Efficiency) (New England Biolabs) as per manufacturer instructions and plated on ampicillin agar plates overnight. Colonies were grown in LB broth with ampicillin and plasmid was purified using NucleoBond Xtra Midi kit (Machery Nagel). Plasmids were confirmed by PCR with the cloning primers above and fragments were gel purified and were confirmed by Sanger sequencing with the forward primer.

Lentivirus production, titration and cell line transduction

ACE2 lentivirus was produced by co-transfection of HEK293T cells with the pCDH-ACE2 plasmid, VSV-G and Gag-Pol using Lipofectamine 2000 Reagent (Thermo Fisher Scientific) or Xfect Transfection Reagent (Takara Bio) as per manufacturer instructions. Supernatant was collected 2 days after transfection and centrifuged at 500 x g for 10 min, and this was concentrated using Amicon Ultra-15 Centrifugal Filter Units with 100 kDa cutoff (Merck Millipore) as per manufacturer instructions. Lentivirus was titrated by serial dilution of lentivirus and incubating with 5000 HEK293T cells in 96 well plates with 8 µg/ml polybrene for 3 days followed by GFP detection by flow cytometry (BD Biosciences LSRFortessa). Transduction units (TU) per ml was calculated by percentage of 5000 cells that are GFP positive multiplied by the dilution. For example if 2 µl lentivirus gives 5% GFP positive cells, the TU/ml is ((5/100)*5000) * (1000/2) = 125,000 TU/ml. The p24 equivalent (ng/ml) was measured using Lenti-X GoStix Plus (Takara Bio) as per manufacturer instructions.
Cell lines were transduced by incubating with lentivirus and 8 µg/ml polybrene for 2-3 days followed by 5 µg/ml puromycin treatment until most resistant cells expressed GFP. Cells were then infected with SARS-CoV-2 at MOI 0.1 for 1 hr at 37◦C, cells were washed with PBS and media replaced. Culture supernatant was harvested at the indicated timepoints and titered by CCID50 assay as described.

UV-inactivated SARS-CoV-2 vaccine preparation and mice vaccination

120 ml of SARS-CoV-2 was inactivated with at least 7650 J/m^2 UVC in a UVC 500 Ultraviolet Crosslinker (Hoefer). Virus was determined to be inactivated by incubation with Vero E6 cells for 4 days without development of CPE. UV-inactive SARS-CoV-2 was then partially-purified using a 20% sucrose cushion centrifuged at 175,000 x g for 3-4 hr using SW32Ti rotor (Beckman Coulter). The sample that has passed through the sucrose was collected and concentrated using Amicon Ultra-15 Centrifugal Filter Units with 100 kDa cutoff (Merck Millipore). For infectious SARS-CoV-2 immunization, virus was also concentrated using Amicon Ultra-15 Centrifugal Filter Units with 100 kDa cutoff (Merck Millipore). Mice were injected s.c. in the base of the tail with 100 ul of UV-inactive or infectious SARS-CoV-2 with 25 ug in 50 ul adjuvant made with the same ingredients as AS01 (Chlibek et al., 2013) as described previously (Yan et al., 2020). A boost was given 5-6 weeks after prime, and mice were bled to measure serum neutralizing titers 4-9 weeks after boost.

Neutralization assay

Mouse serum was heat inactivated at 56◦C for 30 min and incubated with 100 CCID50 SARS-CoV-2 for 2 hr at 37◦C before adding 10^5 Vero cells/well in a 96 well plate to 200 µl. After 4 days cells were fixed and stained by adding 50 µl formaldehyde (15% w/v) and crystal violet (0.1% w/v) (Sigma-Aldrich) overnight. The plates were washed in tap water, dried overnight and 100 µl/well of 100% methanol added to dissolve the crystal violet and the OD was read at 595 nm using a 96-well plate reader (Biotek Synergy H4). The 50% neutralizing titers were interpolated from optical density (OD) versus dilution plots.

Mice intranasal lentivirus transduction and SARS-CoV-2 infection

C57BL/6J, IFNAR$^{-/-}$ (Swann et al., 2007) (originally provided by P. Hertzog, Monash University, Melbourne, VIC, Australia) and IL-28RA$^{-/-}$ (Ank et al., 2008; Galani et al., 2017) mice were bred in-house

at QIMRB. Female mice were 8 weeks to 1 year old (age matched between groups) at the start of the experiment. Mice were anesthetized using isoflurane and 4 µl of 1% L-α-Lysophosphatidylcholine from egg yolk (Sigma Aldrich) in water was administered intranasally. After 1 hour mice were inoculated intranasally with approximately 2×10^4 TU of hACE2-pCDH lentivirus in 50 µl, and 1 week later challenged with 10^5 CCID50 SARS-CoV-2 intranasally in 50 µl. Mice were sacrificed by cervical dislocation at day 2, 4 or 6 and lungs were collected. Superior lobe, middle lobe and inferior lobe of the right lung was immediately homogenized in tubes each containing 4 beads twice at 6000 x g for 15 seconds, and used in tissue titration as described above. Left lung was placed in RNAprotect Tissue Reagent (QIAGEN) at 4◦C overnight then -80◦C. The post-caval lobe of the right lung was fixed in 10% formalin for 4-5 days before transfer to 70% EtOh for histology.
K18-hACE2 mice (McCray et al., 2007) were purchased from The Jackson Laboratory and bred in-house at QIMRB with C57BL/6J mice. Mice were genotyped using Extract-N-Amp Tissue PCR Kit (Sigma Aldrich) according to manufacturer instructions with the following primers; Forward 5'-CTTGGTGATATGTGGGGTAGA-3' and Reverse 5'-CGCTTCATCTCCCACCACTT-3'. hACE2 positive mice were infected with 5×10^4 SARS-CoV-2 i.n. as above and lung RNA was harvested at day 4 for RNA-seq.

RT-qPCR

Mice lung was transferred from RNAlater to TRIzol (Life Technologies) and was homogenized twice at 6000 x g for 15 sec. Homogenates were centrifuged at 14,000 × g for 10 min and RNA was isolated as per manufacturer's instructions. cDNA was synthesized using ProtoScript II First Strand cDNA Synthesis Kit (New England Biolabs) and qPCR performed using iTaq Universal SYBR Green Supermix (Bio-Rad) as per manufacturer instructions with the following primers; SARS-CoV-2 E Forward 5'-ACAGGTACGTTAATAGTTAATAGCGT -3' and Reverse 5'- ATATTGCAGCAGTACGCACACA, hACE2 Forward 5'- GATCACGATTCCCAGGACG -3' and Reverse 5'- TCCGGCTGAACGACAACTC -3', mRPL13a (Schroder et al., 2010) Forward 5'- GAGGTCGGGTGGAAGTACCA -3' and Reverse 3'-TGCATCTTGGCCTTTTCCTT -3'. PCR fragments of SARS-CoV-2 E, ACE2 and mRPL13a using the same primers as above were gel purified and 10-fold serial dilutions of estimated copy numbers were used as standards in qPCR to calculate copies in samples reactions. SARS-CoV-2 E and ACE2 copies were normalized by mRPL13a copy number in each reaction. qPCR reactions were performed in duplicate and averaged to determine the copy number in each reaction.

RNAseq

TRIzol extracted lung RNA was treated with DNase (RNAseq-Free DNAse Set (Qiagen)) followed by purification using RNeasy MinElute Cleanup Kit (QIAGEN) as per manufacturer instructions. RNA concentration and quality was measured using TapeStation D1K TapeScreen assay (Agilent). cDNA libraries were prepared using the Illumina TruSeq Stranded mRNA library prep kit and the sequencing performed on the Illumina Nextseq 550 platform generating 75bp paired end reads. Per base sequence quality for >90% bases was above Q30 for all samples. The quality of raw sequencing reads was assessed using FastQC (Simons, 2010) (v0.11.8) and trimmed using Cutadapt (Martin, 2011) (v2.3) to remove adapter sequences and low-quality bases. Trimmed reads were aligned using STAR (Dobin et al., 2013) (v2.7.1a) to a combined reference that included the mouse GRCm38 primary assembly and the GENCODE M23 gene model (Harrow et al., 2012), SARS-CoV-2 isolate Wuhan-Hu-1 (NC_045512.2; 29903 bp) and the human ACE2 mouse codon optimized sequence (2418 bp). Mouse gene expression was estimated using RSEM (Li and Dewey, 2011) (v1.3.0). Reads aligned to SARS-CoV-2 and hACE2 were counted using SAMtools (Li et al., 2009) (v1.9). Differential gene expression in the mouse was analyzed using EdgeR (3.22.3) and modelled using the likelihood ratio test, glmLRT().

Analyses of K18-hACE2 and Ad5-hACE2 RNA-seq data

RNA-seq datasets generated from the Winkler et al. study (Winkler et al., 2020), and Sun et al. study (Sun et al., 2020a) were obtained from the Gene Expression Omnibus (GSE154104 and GSE150847 respectively) and trimmed using Cutadapt (v2.3). Trimmed reads were aligned using STAR (v2.7.1a) to a combined reference that included the mouse GRCm38 primary assembly and the GENCODE M23 gene model, SARS-CoV-2 isolate Wuhan-Hu-1 (NC_045512.2; 29903 bp) and the human ACE2 transcript variant 1 (NM_001371415.1; 3339 bp). Mouse gene expression was estimated using RSEM (v1.3.0). Reads aligned to SARS-CoV-2 and hACE2 were counted using SAMtools (v1.9). Differential gene expression in the mouse was analyzed using EdgeR (3.22.3) and modelled using the likelihood ratio test, glmLRT().

Pathway Analysis

Up-Stream Regulators (USR), Diseases and Functions and canonical pathways enriched in differentially expressed genes in direct and indirect interactions were investigated using Ingenuity Pathway Analysis (IPA) (QIAGEN).

Network Analysis

Protein interaction networks of differentially expressed gene lists were visualized in Cytoscape (v3.7.2) (Shannon et al., 2003). Enrichment for biological processes, molecular functions, KEGG pathways and other gene ontology categories in DEG lists was elucidated using the STRING database (Szklarczyk et al., 2019) and GO enrichment analysis (Mi et al., 2019).

Gene Set Enrichment Analysis

Preranked GSEA (Subramanian et al., 2005) was performed on a desktop application (GSEA v4.0.3) (http://www.broadinstitute.org/gsea/) using the "GSEAPreranked" module. Gene sets from the supplemental materials from the Winkler et al. (Winkler et al., 2020), Blanco-Melo et al. (Blanco-Melo et al., 2020) and Wu et al. (Wu et al., 2020b) (filename.GMT) studies were investigated for enrichment in our pre-ranked all gene list for SARS-CoV-2 infected day 2 mice lung comparing plus versus minus ACE2 (Supplementary Table 2B). Li et al. (Li et al., 2014) blood transcription modules (BTM_for_GSEA_20131008.gmt, n = 346) was also used in GSEA to determine enrichment in our 'vaccinated' versus unvaccinated mice lung at day 2 (Supplementary Table 5B). The complete Molecular Signatures Database (MSigDB) v7.2 gene set collection (31,120 gene sets) (msigdb.v7.2.symbols.gmt: https://www.gsea-msigdb.org/gsea/msigdb/download_file.jsp?filePath=/msigdb/release/7.2/msigdb.v7.2.symbols.gmt) was used to run GSEAs on pre-ranked gene list for plus versus minus ACE2 at day 2 (Supplementary Table 2B). Gene ontology (Ashburner et al., 2000; Consortium, 2021) and Enrichr (Chen et al., 2013; Kuleshov et al., 2016) web-tools were also consulted.

Interferome

The indicated DEG lists were entered into Interferome (www.interferome.org) (Rusinova et al., 2013) with the following parameters: *In Vivo*, Mus musculus, fold change 2 (up and down).

SUPPPLEMENTAL INFORMATION

Supplementary Figure 1. Replication of SARS-CoV-2 in hACE2-lentivirus transduced mouse cell lines. Growth kinetics of SARS-CoV-2 over a three day time course in untransduced or hACE2-lentivirus transduced 3T3 or AE17 cells infected at MOI=0.1. Data is the mean of triplicate wells and error bars

represent SEM. Images of cells were taken using an inverted light microscope at day 3 post-infection and are representative of triplicate wells.

Supplementary Figure 2. RT-qPCR of mice lung RNA using primers for SARS-CoV-2 normalized to hACE2 introduced by lentivirus transduction. Data is individual mice and is expressed as RNA copy number calculated against a standard curve for each gene.

Supplementary Figure 3. SARS-CoV-2 and hACE2 read counts in RNA-Seq data. RNA-Seq was performed on mice lung from the same mice as in 'Figure 2'. **A)** SARS-CoV-2 read counts normalized to total read count. Data points below the horizontal dotted line had read counts of zero. **B)** hACE2 read counts normalised to total read count. Data points below the horizontal dotted line had read counts of zero. **C)** SARS-CoV-2 read count normalised to hACE2 read count. Circle with pink dotted outline had hACE2 read count of 0, so the value was set to the SARS-CoV-2 read count (not normalised). **D)** SARS-CoV-2 reads aligned to reference genome viewed in Integrative Genome Viewer (IGV). Mice with hACE2 displayed reads mapped across the entire genome, with higher counts for structural gene sub-genomic RNA as also evident in hACE2-adenoviral vector transduced cell lines (Blanco-Melo et al., 2020).

Supplementary Table 1. RNA-Seq gene lists and downstream bioinformatic analyses of responses at day 2 post-infection.

Supplementary Table 2. RNA-Seq gene lists and downstream bioinformatic analyses of responses at day 6 post-infection.

Supplementary Table 3. RNA-Seq gene lists and downstream bioinformatic analyses of responses in IFNAR$^{-/-}$ vs C57BL/6J mice at day 2 post-infection.

Supplementary Table 4. RNA-Seq gene lists and downstream bioinformatic analyses of responses in IL-28RA$^{-/-}$ vs C57BL/6J mice at day 2 post-infection.

Supplementary Table 5. RNA-Seq gene lists and downstream bioinformatic analyses of responses in immunized vs unvaccinated mice at day 2 post-infection.

REFERENCES

Alexander, M.R., Schoeder, C.T., Brown, J.A., Smart, C.D., Moth, C., Wikswo, J.P., Capra, J.A., Meiler, J., Chen, W., and Madhur, M.S. (2020). Predicting susceptibility to SARS-CoV-2 infection based on structural differences in ACE2 across species. The FASEB Journal *34*, 15946-15960.

Alton, E.W., Beekman, J.M., Boyd, A.C., Brand, J., Carlon, M.S., Connolly, M.M., Chan, M., Conlon, S., Davidson, H.E., Davies, J.C., *et al.* (2017a). Preparation for a first-in-man lentivirus trial in patients with cystic fibrosis. Thorax *72*, 137-147.

Alton, E.W.F.W., Beekman, J.M., Boyd, A.C., Brand, J., Carlon, M.S., Connolly, M.M., Chan, M., Conlon, S., Davidson, H.E., Davies, J.C., *et al.* (2017b). Preparation for a first-in-man lentivirus trial in patients with cystic fibrosis. Thorax *72*, 137.

Ank, N., Iversen, M.B., Bartholdy, C., Staeheli, P., Hartmann, R., Jensen, U.B., Dagnaes-Hansen, F., Thomsen, A.R., Chen, Z., Haugen, H., *et al.* (2008). An Important Role for Type III Interferon (IFN-λ/IL-28) in TLR-Induced Antiviral Activity. The Journal of Immunology *180*, 2474-2485.

797 Ashburner, M., Ball, C.A., Blake, J.A., Botstein, D., Butler, H., Cherry, J.M., Davis, A.P., Dolinski, K., Dwight,
798 S.S., Eppig, J.T., *et al.* (2000). Gene ontology: tool for the unification of biology. The Gene Ontology
799 Consortium. Nature genetics *25*, 25-29.
800 Badawy, A.A.B. (2020). Immunotherapy of COVID-19 with poly (ADP-ribose) polymerase inhibitors:
801 starting with nicotinamide. Biosci Rep *40*, BSR20202856.
802 Banerjee, A.K., Blanco, M.R., Bruce, E.A., Honson, D.D., Chen, L.M., Chow, A., Bhat, P., Ollikainen, N.,
803 Quinodoz, S.A., Loney, C., *et al.* (2020). SARS-CoV-2 Disrupts Splicing, Translation, and Protein Trafficking
804 to Suppress Host Defenses. Cell *183*, 1325-1339.e1321.
805 Bao, L., Deng, W., Huang, B., Gao, H., Liu, J., Ren, L., Wei, Q., Yu, P., Xu, Y., Qi, F., *et al.* (2020). The
806 pathogenicity of SARS-CoV-2 in hACE2 transgenic mice. Nature *583*, 830-833.
807 Blanco-Melo, D., Nilsson-Payant, B.E., Liu, W.C., Uhl, S., Hoagland, D., Møller, R., Jordan, T.X., Oishi, K.,
808 Panis, M., Sachs, D., *et al.* (2020). Imbalanced Host Response to SARS-CoV-2 Drives Development of
809 COVID-19. Cell *181*, 1036-1045.e1039.
810 Boudewijns, R., Thibaut, H.J., Kaptein, S.J.F., Li, R., Vergote, V., Seldeslachts, L., Van Weyenbergh, J., De
811 Keyzer, C., Bervoets, L., Sharma, S., *et al.* (2020). STAT2 signaling restricts viral dissemination but drives
812 severe pneumonia in SARS-CoV-2 infected hamsters. Nature Communications *11*, 5838.
813 Buckley, S.M.K., Howe, S.J., Sheard, V., Ward, N.J., Coutelle, C., Thrasher, A.J., Waddington, S.N., and
814 McKay, T.R. (2008). Lentiviral transduction of the murine lung provides efficient pseudotype and
815 developmental stage-dependent cell-specific transgene expression. Gene Therapy *15*, 1167-1175.
816 Carossino, M., Montanaro, P., O'Connell, A., Kenney, D., Gertje, H., Grosz, K.A., Kurnick, S.A., Bosmann,
817 M., Saeed, M., Balasuriya, U.B.R., *et al.* (2021). Fatal neuroinvasion of SARS-CoV-2 in K18-hACE2 mice is
818 partially dependent on hACE2 expression. bioRxiv.
819 Chan, K.K., Dorosky, D., Sharma, P., Abbasi, S.A., Dye, J.M., Kranz, D.M., Herbert, A.S., and Procko, E.
820 (2020). Engineering human ACE2 to optimize binding to the spike protein of SARS coronavirus 2. Science
821 (New York, NY) *369*, 1261-1265.
822 Channappanavar, R., Fehr, Anthony R., Vijay, R., Mack, M., Zhao, J., Meyerholz, David K., and Perlman, S.
823 (2016). Dysregulated Type I Interferon and Inflammatory Monocyte-Macrophage Responses Cause
824 Lethal Pneumonia in SARS-CoV-Infected Mice. Cell host & microbe *19*, 181-193.
825 Channappanavar, R., Fett, C., Mack, M., Ten Eyck, P.P., Meyerholz, D.K., and Perlman, S. (2017). Sex-
826 Based Differences in Susceptibility to Severe Acute Respiratory Syndrome Coronavirus Infection. J
827 Immunol *198*, 4046-4053.
828 Chen, E.Y., Tan, C.M., Kou, Y., Duan, Q., Wang, Z., Meirelles, G.V., Clark, N.R., and Ma'ayan, A. (2013).
829 Enrichr: interactive and collaborative HTML5 gene list enrichment analysis tool. BMC Bioinformatics *14*,
830 128.
831 Chlibek, R., Bayas, J.M., Collins, H., de la Pinta, M.L.R., Ledent, E., Mols, J.F., and Heineman, T.C. (2013).
832 Safety and Immunogenicity of an AS01-adjuvanted Varicella-zoster Virus Subunit Candidate Vaccine
833 Against Herpes Zoster in Adults ≥50 Years of Age. The Journal of Infectious Diseases *208*, 1953-1961.
834 Consortium, G.O. (2021). The Gene Ontology resource: enriching a GOld mine. Nucleic Acids Res *49*,
835 D325-d334.
836 Copreni, E., Palmieri, L., Castellani, S., and Conese, M. (2010). A VSV-G Pseudotyped Last Generation
837 Lentiviral Vector Mediates High Level and Persistent Gene Transfer in Models of Airway Epithelium In
838 Vitro and In Vivo. Viruses *2*, 1577-1588.
839 Copreni, E., Penzo, M., Carrabino, S., and Conese, M. (2004). Lentivirus-mediated gene transfer to the
840 respiratory epithelium: a promising approach to gene therapy of cystic fibrosis. Gene Therapy *11*, S67-
841 S75.
842 Crawford, K.H.D., Eguia, R., Dingens, A.S., Loes, A.N., Malone, K.D., Wolf, C.R., Chu, H.Y., Tortorici, M.A.,
843 Veesler, D., Murphy, M., *et al.* (2020). Protocol and Reagents for Pseudotyping Lentiviral Particles with
844 SARS-CoV-2 Spike Protein for Neutralization Assays. Viruses *12*.

845 Curtin, N., Bányai, K., Thaventhiran, J., Le Quesne, J., Helyes, Z., and Bai, P. (2020). Repositioning PARP
846 inhibitors for SARS-CoV-2 infection(COVID-19); a new multi-pronged therapy for acute respiratory
847 distress syndrome? British Journal of Pharmacology *177*, 3635-3645.
848 Damas, J., Hughes, G.M., Keough, K.C., Painter, C.A., Persky, N.S., Corbo, M., Hiller, M., Koepfli, K.-P.,
849 Pfenning, A.R., Zhao, H.*, et al.* (2020). Broad host range of SARS-CoV-2 predicted by comparative and
850 structural analysis of ACE2 in vertebrates. Proceedings of the National Academy of Sciences *117*, 22311-
851 22322.
852 Dinnon, K.H., Leist, S.R., Schäfer, A., Edwards, C.E., Martinez, D.R., Montgomery, S.A., West, A., Yount,
853 B.L., Hou, Y.J., Adams, L.E.*, et al.* (2020). A mouse-adapted model of SARS-CoV-2 to test COVID-19
854 countermeasures. Nature *586*, 560-566.
855 Dobin, A., Davis, C.A., Schlesinger, F., Drenkow, J., Zaleski, C., Jha, S., Batut, P., Chaisson, M., and
856 Gingeras, T.R. (2013). STAR: ultrafast universal RNA-seq aligner. Bioinformatics *29*, 15-21.
857 Duperray, C., Boiron, J.M., Boucheix, C., Cantaloube, J.F., Lavabre-Bertrand, T., Attal, M., Brochier, J.,
858 Maraninchi, D., Bataille, R., and Klein, B. (1990). The CD24 antigen discriminates between pre-B and B
859 cells in human bone marrow. J Immunol *145*, 3678-3683.
860 Felgenhauer, U., Schoen, A., Gad, H.H., Hartmann, R., Schaubmar, A.R., Failing, K., Drosten, C., and
861 Weber, F. (2020). Inhibition of SARS-CoV-2 by type I and type III interferons. J Biol Chem *295*, 13958-
862 13964.
863 Frieman, M.B., Chen, J., Morrison, T.E., Whitmore, A., Funkhouser, W., Ward, J.M., Lamirande, E.W.,
864 Roberts, A., Heise, M., Subbarao, K.*, et al.* (2010). SARS-CoV Pathogenesis Is Regulated by a STAT1
865 Dependent but a Type I, II and III Interferon Receptor Independent Mechanism. PLOS Pathogens *6*,
866 e1000849.
867 Gadotti, A.C., de Castro Deus, M., Telles, J.P., Wind, R., Goes, M., Garcia Charello Ossoski, R., de Padua,
868 A.M., de Noronha, L., Moreno-Amaral, A., Baena, C.P.*, et al.* (2020). IFN-γ is an independent risk factor
869 associated with mortality in patients with moderate and severe COVID-19 infection. Virus Res *289*,
870 198171-198171.
871 Galani, I.E., Triantafyllia, V., Eleminiadou, E.E., Koltsida, O., Stavropoulos, A., Manioudaki, M., Thanos, D.,
872 Doyle, S.E., Kotenko, S.V., Thanopoulou, K.*, et al.* (2017). Interferon-λ Mediates Non-redundant Front-
873 Line Antiviral Protection against Influenza Virus Infection without Compromising Host Fitness. Immunity
874 *46*, 875-890.e876.
875 Golden, J.W., Cline, C.R., Zeng, X., Garrison, A.R., Carey, B.D., Mucker, E.M., White, L.E., Shamblin, J.D.,
876 Brocato, R.L., Liu, J.*, et al.* (2020). Human angiotensin-converting enzyme 2 transgenic mice infected with
877 SARS-CoV-2 develop severe and fatal respiratory disease. JCI insight.
878 Griffin, B.D., Chan, M., Tailor, N., Mendoza, E.J., Leung, A., Warner, B.M., Duggan, A.T., Moffat, E., He, S.,
879 Garnett, L.*, et al.* (2020). North American deer mice are susceptible to SARS-CoV-2. bioRxiv,
880 2020.2007.2025.221291.
881 Gu, H., Chen, Q., Yang, G., He, L., Fan, H., Deng, Y.-Q., Wang, Y., Teng, Y., Zhao, Z., Cui, Y.*, et al.* (2020).
882 Adaptation of SARS-CoV-2 in BALB/c mice for testing vaccine efficacy. Science (New York, NY) *369*, 1603-
883 1607.
884 Guan, W.-j., Ni, Z.-y., Hu, Y., Liang, W.-h., Ou, C.-q., He, J.-x., Liu, L., Shan, H., Lei, C.-l., Hui, D.S.C.*, et al.*
885 (2020). Clinical Characteristics of Coronavirus Disease 2019 in China. New England Journal of Medicine
886 *382*, 1708-1720.
887 Han, H., Ma, Q., Li, C., Liu, R., Zhao, L., Wang, W., Zhang, P., Liu, X., Gao, G., Liu, F.*, et al.* (2020). Profiling
888 serum cytokines in COVID-19 patients reveals IL-6 and IL-10 are disease severity predictors. Emerging
889 microbes & infections *9*, 1123-1130.
890 Harrow, J., Frankish, A., Gonzalez, J.M., Tapanari, E., Diekhans, M., Kokocinski, F., Aken, B.L., Barrell, D.,
891 Zadissa, A., Searle, S.*, et al.* (2012). GENCODE: the reference human genome annotation for The ENCODE
892 Project. Genome Res *22*, 1760-1774.

893 Hassan, A.O., Case, J.B., Winkler, E.S., Thackray, L.B., Kafai, N.M., Bailey, A.L., McCune, B.T., Fox, J.M.,
894 Chen, R.E., Alsoussi, W.B., *et al.* (2020). A SARS-CoV-2 Infection Model in Mice Demonstrates Protection
895 by Neutralizing Antibodies. Cell *182*, 744-753.e744.
896 Herold, T., Jurinovic, V., Arnreich, C., Lipworth, B.J., Hellmuth, J.C., von Bergwelt-Baildon, M., Klein, M.,
897 and Weinberger, T. (2020). Elevated levels of IL-6 and CRP predict the need for mechanical ventilation in
898 COVID-19. Journal of Allergy and Clinical Immunology *146*, 128-136.e124.
899 Huang, C., Wang, Y., Li, X., Ren, L., Zhao, J., Hu, Y., Zhang, L., Fan, G., Xu, J., Gu, X., *et al.* (2020). Clinical
900 features of patients infected with 2019 novel coronavirus in Wuhan, China. Lancet (London, England)
901 *395*, 497-506.
902 Israelow, B., Song, E., Mao, T., Lu, P., Meir, A., Liu, F., Alfajaro, M.M., Wei, J., Dong, H., Homer, R.J., *et al.*
903 (2020). Mouse model of SARS-CoV-2 reveals inflammatory role of type I interferon signaling. The Journal
904 of experimental medicine *217*.
905 Jefferson, T., Spencer, E., Brassey, J., and Heneghan, C. (2020). Viral cultures for COVID-19 infectivity
906 assessment. Systematic review. medRxiv, 2020.2008.2004.20167932.
907 Jiang, H.-w., Zhang, H.-n., Meng, Q.-f., Xie, J., Li, Y., Chen, H., Zheng, Y.-x., Wang, X.-n., Qi, H., Zhang, J., *et*
908 *al.* (2020a). SARS-CoV-2 Orf9b suppresses type I interferon responses by targeting TOM70. Cellular &
909 Molecular Immunology *17*, 998-1000.
910 Jiang, R.-D., Liu, M.-Q., Chen, Y., Shan, C., Zhou, Y.-W., Shen, X.-R., Li, Q., Zhang, L., Zhu, Y., Si, H.-R., *et al.*
911 (2020b). Pathogenesis of SARS-CoV-2 in Transgenic Mice Expressing Human Angiotensin-Converting
912 Enzyme 2. Cell *182*, 50-58.e58.
913 Jin, J.-M., Bai, P., He, W., Wu, F., Liu, X.-F., Han, D.-M., Liu, S., and Yang, J.-K. (2020). Gender Differences
914 in Patients With COVID-19: Focus on Severity and Mortality. Frontiers in Public Health *8*.
915 Johnson, B.J., Le, T.T., Dobbin, C.A., Banovic, T., Howard, C.B., Flores Fde, M., Vanags, D., Naylor, D.J.,
916 Hill, G.R., and Suhrbier, A. (2005). Heat shock protein 10 inhibits lipopolysaccharide-induced
917 inflammatory mediator production. J Biol Chem *280*, 4037-4047.
918 Kremer, K.L., Dunning, K.R., Parsons, D.W., and Anson, D.S. (2007). Gene delivery to airway epithelial
919 cells in vivo: a direct comparison of apical and basolateral transduction strategies using pseudotyped
920 lentivirus vectors. The journal of gene medicine *9*, 362-368.
921 Kuleshov, M.V., Jones, M.R., Rouillard, A.D., Fernandez, N.F., Duan, Q., Wang, Z., Koplev, S., Jenkins, S.L.,
922 Jagodnik, K.M., Lachmann, A., *et al.* (2016). Enrichr: a comprehensive gene set enrichment analysis web
923 server 2016 update. Nucleic Acids Res *44*, W90-97.
924 Kumari, P., Rothan, H.A., Natekar, J.P., Stone, S., Pathak, H., Strate, P.G., Arora, K., Brinton, M.A., and
925 Kumar, M. (2020). Neuroinvasion and encephalitis following intranasal inoculation of SARS-CoV-2 in K18-
926 hACE2 mice. bioRxiv, 2020.2012.2014.422714.
927 La Linn, M., Bellett, A.J., Parsons, P.G., and Suhrbier, A. (1995). Complete removal of mycoplasma from
928 viral preparations using solvent extraction. J Virol Methods *52*, 51-54.
929 Lavoie, H., Gagnon, J., and Therrien, M. (2020). ERK signalling: a master regulator of cell behaviour, life
930 and fate. Nature Reviews Molecular Cell Biology *21*, 607-632.
931 Lazear, H.M., Schoggins, J.W., and Diamond, M.S. (2019). Shared and Distinct Functions of Type I and
932 Type III Interferons. Immunity *50*, 907-923.
933 Leist, S.R., Dinnon, K.H., 3rd, Schäfer, A., Tse, L.V., Okuda, K., Hou, Y.J., West, A., Edwards, C.E., Sanders,
934 W., Fritch, E.J., *et al.* (2020). A Mouse-Adapted SARS-CoV-2 Induces Acute Lung Injury and Mortality in
935 Standard Laboratory Mice. Cell.
936 Li, B., and Dewey, C.N. (2011). RSEM: accurate transcript quantification from RNA-Seq data with or
937 without a reference genome. BMC Bioinformatics *12*, 323.
938 Li, H., Handsaker, B., Wysoker, A., Fennell, T., Ruan, J., Homer, N., Marth, G., Abecasis, G., and Durbin, R.
939 (2009). The Sequence Alignment/Map format and SAMtools. Bioinformatics *25*, 2078-2079.

940 Li, S., Rouphael, N., Duraisingham, S., Romero-Steiner, S., Presnell, S., Davis, C., Schmidt, D.S., Johnson,
941 S.E., Milton, A., Rajam, G.*, et al.* (2014). Molecular signatures of antibody responses derived from a
942 systems biology study of five human vaccines. Nature immunology *15*, 195-204.
943 Limberis, M., Anson, D.S., Fuller, M., and Parsons, D.W. (2002). Recovery of airway cystic fibrosis
944 transmembrane conductance regulator function in mice with cystic fibrosis after single-dose lentivirus-
945 mediated gene transfer. Human gene therapy *13*, 1961-1970.
946 Limberis, M.P., Bell, C.L., Heath, J., and Wilson, J.M. (2010). Activation of transgene-specific T cells
947 following lentivirus-mediated gene delivery to mouse lung. Mol Ther *18*, 143-150.
948 Lin, L., Han, Q., Xiong, Y., Li, T., Liu, Z., Xu, H., Wu, Y., Wang, N., and Liu, X. (2017). Krüpple-like-factor 4
949 Attenuates Lung Fibrosis via Inhibiting Epithelial-mesenchymal Transition. Scientific reports *7*, 15847-
950 15847.
951 Lu, L., Zhang, H., Dauphars, D.J., and He, Y.-W. (2021). A Potential Role of Interleukin 10 in COVID-19
952 Pathogenesis. Trends in Immunology *42*, 3-5.
953 Mahlakõiv, T., Ritz, D., Mordstein, M., DeDiego, M.L., Enjuanes, L., Müller, M.A., Drosten, C., and
954 Staeheli, P. (2012). Combined action of type I and type III interferon restricts initial replication of severe
955 acute respiratory syndrome coronavirus in the lung but fails to inhibit systemic virus spread. The Journal
956 of general virology *93*, 2601-2605.
957 Martin, M. (2011). Cutadapt removes adapter sequences from high-throughput sequencing reads. 2011
958 *17*, 3.
959 Masiá, M., Fernández-González, M., Padilla, S., Ortega, P., García, J.A., Agulló, V., García-Abellán, J.,
960 Telenti, G., Guillén, L., and Gutiérrez, F. (2020). Impact of interleukin-6 blockade with tocilizumab on
961 SARS-CoV-2 viral kinetics and antibody responses in patients with COVID-19: A prospective cohort study.
962 EBioMedicine *60*.
963 McCray, P.B., Jr., Pewe, L., Wohlford-Lenane, C., Hickey, M., Manzel, L., Shi, L., Netland, J., Jia, H.P.,
964 Halabi, C., Sigmund, C.D.*, et al.* (2007). Lethal infection of K18-hACE2 mice infected with severe acute
965 respiratory syndrome coronavirus. Journal of virology *81*, 813-821.
966 Mehdipour, A.R., and Hummer, G. (2020). Dual nature of human ACE2 glycosylation in binding to SARS-
967 CoV-2 spike. bioRxiv, 2020.2007.2009.193680.
968 Mi, H., Muruganujan, A., Ebert, D., Huang, X., and Thomas, P.D. (2019). PANTHER version 14: more
969 genomes, a new PANTHER GO-slim and improvements in enrichment analysis tools. Nucleic Acids Res *47*,
970 D419-d426.
971 Miller, B., Silverstein, A., Flores, M., Cao, K., Kumagai, H., Mehta, H.H., Yen, K., Kim, S.-J., and Cohen, P.
972 (2021). Host mitochondrial transcriptome response to SARS-CoV-2 in multiple cell models and clinical
973 samples. Scientific Reports *11*, 3.
974 Miorin, L., Kehrer, T., Sanchez-Aparicio, M.T., Zhang, K., Cohen, P., Patel, R.S., Cupic, A., Makio, T., Mei,
975 M., Moreno, E.*, et al.* (2020). SARS-CoV-2 Orf6 hijacks Nup98 to block STAT nuclear import and
976 antagonize interferon signaling. Proceedings of the National Academy of Sciences *117*, 28344.
977 Monk, P.D., Marsden, R.J., Tear, V.J., Brookes, J., Batten, T.N., Mankowski, M., Gabbay, F.J., Davies, D.E.,
978 Holgate, S.T., Ho, L.-P.*, et al.* (2020). Safety and efficacy of inhaled nebulised interferon beta-1a
979 (SNG001) for treatment of SARS-CoV-2 infection: a randomised, double-blind, placebo-controlled, phase
980 2 trial. The Lancet Respiratory Medicine.
981 Moreau, G.B., Burgess, S.L., Sturek, J.M., Donlan, A.N., Petri, W.A., and Mann, B.J. (2020). Evaluation of
982 K18-hACE2 Mice as a Model of SARS-CoV-2 Infection. The American journal of tropical medicine and
983 hygiene *103*, 1215-1219.
984 Muñoz-Fontela, C., Dowling, W.E., Funnell, S.G.P., Gsell, P.-S., Riveros-Balta, A.X., Albrecht, R.A.,
985 Andersen, H., Baric, R.S., Carroll, M.W., Cavaleri, M.*, et al.* (2020). Animal models for COVID-19. Nature
986 *586*, 509-515.

987 Nechanitzky, R., Akbas, D., Scherer, S., Györy, I., Hoyler, T., Ramamoorthy, S., Diefenbach, A., and
988 Grosschedl, R. (2013). Transcription factor EBF1 is essential for the maintenance of B cell identity and
989 prevention of alternative fates in committed cells. Nature immunology *14*, 867-875.
990 Nicks, K.M., Fowler, T.W., Akel, N.S., Perrien, D.S., Suva, L.J., and Gaddy, D. (2010). Bone turnover across
991 the menopause transition : The role of gonadal inhibins. Ann N Y Acad Sci *1192*, 153-160.
992 Oladunni, F.S., Park, J.-G., Pino, P.A., Gonzalez, O., Akhter, A., Allué-Guardia, A., Olmo-Fontánez, A.,
993 Gautam, S., Garcia-Vilanova, A., Ye, C.*, et al.* (2020). Lethality of SARS-CoV-2 infection in K18 human
994 angiotensin-converting enzyme 2 transgenic mice. Nature Communications *11*, 6122.
995 Peckham, H., de Gruijter, N.M., Raine, C., Radziszewska, A., Ciurtin, C., Wedderburn, L.R., Rosser, E.C.,
996 Webb, K., and Deakin, C.T. (2020). Male sex identified by global COVID-19 meta-analysis as a risk factor
997 for death and ITU admission. Nature Communications *11*, 6317.
998 Pinna, G. (2021). Sex and COVID-19: A Protective Role for Reproductive Steroids. Trends in
999 endocrinology and metabolism: TEM *32*, 3-6.
1000 Raslan, A.A., and Yoon, J.K. (2020). WNT Signaling in Lung Repair and Regeneration. Mol Cells *43*, 774-
1001 783.
1002 Rathnasinghe, R., Strohmeier, S., Amanat, F., Gillespie, V.L., Krammer, F., García-Sastre, A., Coughlan, L.,
1003 Schotsaert, M., and Uccellini, M. (2020). Comparison of Transgenic and Adenovirus hACE2 Mouse
1004 Models for SARS-CoV-2 Infection. Emerging microbes & infections, 1-19.
1005 Rodrigues, J.P.G.L.M., Barrera-Vilarmau, S., M. C. Teixeira, J., Sorokina, M., Seckel, E., Kastritis, P.L., and
1006 Levitt, M. (2020). Insights on cross-species transmission of SARS-CoV-2 from structural modeling. PLOS
1007 Computational Biology *16*, e1008449.
1008 Rusinova, I., Forster, S., Yu, S., Kannan, A., Masse, M., Cumming, H., Chapman, R., and Hertzog, P.J.
1009 (2013). INTERFEROME v2.0: an updated database of annotated interferon-regulated genes. Nucleic Acids
1010 Research *41*, D1040-D1046.
1011 Schroder, W.A., Le, T.T.T., Major, L., Street, S., Gardner, J., Lambley, E., Markey, K., MacDonald, K.P.,
1012 Fish, R.J., Thomas, R.*, et al.* (2010). A Physiological Function of Inflammation-Associated SerpinB2 Is
1013 Regulation of Adaptive Immunity. The Journal of Immunology *184*, 2663.
1014 Schubert, K., Karousis, E.D., Jomaa, A., Scaiola, A., Echeverria, B., Gurzeler, L.-A., Leibundgut, M., Thiel,
1015 V., Mühlemann, O., and Ban, N. (2020). SARS-CoV-2 Nsp1 binds the ribosomal mRNA channel to inhibit
1016 translation. Nature Structural & Molecular Biology *27*, 959-966.
1017 Shannon, P., Markiel, A., Ozier, O., Baliga, N.S., Wang, J.T., Ramage, D., Amin, N., Schwikowski, B., and
1018 Ideker, T. (2003). Cytoscape: a software environment for integrated models of biomolecular interaction
1019 networks. Genome Res *13*, 2498-2504.
1020 Simons, A. (2010). A quality control tool for high throughput sequence data. Available online:
1021 https://www.bioinformatics.babraham.ac.uk/projects/fastqc.
1022 Sountoulidis, A., Stavropoulos, A., Giaglis, S., Apostolou, E., Monteiro, R., Chuva de Sousa Lopes, S.M.,
1023 Chen, H., Stripp, B.R., Mummery, C., Andreakos, E.*, et al.* (2012). Activation of the Canonical Bone
1024 Morphogenetic Protein (BMP) Pathway during Lung Morphogenesis and Adult Lung Tissue Repair. PLOS
1025 ONE *7*, e41460.
1026 Subramanian, A., Tamayo, P., Mootha, V.K., Mukherjee, S., Ebert, B.L., Gillette, M.A., Paulovich, A.,
1027 Pomeroy, S.L., Golub, T.R., Lander, E.S.*, et al.* (2005). Gene set enrichment analysis: a knowledge-based
1028 approach for interpreting genome-wide expression profiles. Proc Natl Acad Sci U S A *102*, 15545-15550.
1029 Sun, J., Zhuang, Z., Zheng, J., Li, K., Wong, R.L.-Y., Liu, D., Huang, J., He, J., Zhu, A., Zhao, J.*, et al.* (2020a).
1030 Generation of a Broadly Useful Model for COVID-19 Pathogenesis, Vaccination, and Treatment. Cell *182*,
1031 734-743.e735.
1032 Sun, S.H., Chen, Q., Gu, H.J., Yang, G., Wang, Y.X., Huang, X.Y., Liu, S.S., Zhang, N.N., Li, X.F., Xiong, R.*, et*
1033 *al.* (2020b). A Mouse Model of SARS-CoV-2 Infection and Pathogenesis. Cell host & microbe *28*, 124-
1034 133.e124.

1035 Swann, J.B., Hayakawa, Y., Zerafa, N., Sheehan, K.C., Scott, B., Schreiber, R.D., Hertzog, P., and Smyth,
1036 M.J. (2007). Type I IFN contributes to NK cell homeostasis, activation, and antitumor function. J Immunol
1037 *178*, 7540-7549.
1038 Szklarczyk, D., Gable, A.L., Lyon, D., Junge, A., Wyder, S., Huerta-Cepas, J., Simonovic, M., Doncheva,
1039 N.T., Morris, J.H., Bork, P.*, et al.* (2019). STRING v11: protein-protein association networks with increased
1040 coverage, supporting functional discovery in genome-wide experimental datasets. Nucleic Acids Res *47*,
1041 D607-D613.
1042 Takasuka, N., Fujii, H., Takahashi, Y., Kasai, M., Morikawa, S., Itamura, S., Ishii, K., Sakaguchi, M., Ohnishi,
1043 K., Ohshima, M.*, et al.* (2004). A subcutaneously injected UV-inactivated SARS coronavirus vaccine elicits
1044 systemic humoral immunity in mice. International immunology *16*, 1423-1430.
1045 Tseng, C.T., Huang, C., Newman, P., Wang, N., Narayanan, K., Watts, D.M., Makino, S., Packard, M.M.,
1046 Zaki, S.R., Chan, T.S.*, et al.* (2007). Severe acute respiratory syndrome coronavirus infection of mice
1047 transgenic for the human Angiotensin-converting enzyme 2 virus receptor. Journal of virology *81*, 1162-
1048 1173.
1049 Vanderheiden, A., Ralfs, P., Chirkova, T., Upadhyay, A.A., Zimmerman, M.G., Bedoya, S., Aoued, H.,
1050 Tharp, G.M., Pellegrini, K.L., Manfredi, C.*, et al.* (2020). Type I and Type III Interferons Restrict SARS-CoV-
1051 2 Infection of Human Airway Epithelial Cultures. Journal of virology *94*, e00985-00920.
1052 Vaz de Paula, C.B., de Azevedo, M.L.V., Nagashima, S., Martins, A.P.C., Malaquias, M.A.S., Miggiolaro,
1053 A.F.R.d.S., da Silva Motta Júnior, J., Avelino, G., do Carmo, L.A.P., Carstens, L.B.*, et al.* (2020). IL-4/IL-13
1054 remodeling pathway of COVID-19 lung injury. Scientific Reports *10*, 18689.
1055 Wajnberg, A., Amanat, F., Firpo, A., Altman, D.R., Bailey, M.J., Mansour, M., McMahon, M., Meade, P.,
1056 Mendu, D.R., Muellers, K.*, et al.* (2020). Robust neutralizing antibodies to SARS-CoV-2 infection persist
1057 for months. Science (New York, NY) *370*, 1227.
1058 Wang, H., Kadlecek, T.A., Au-Yeung, B.B., Goodfellow, H.E.S., Hsu, L.-Y., Freedman, T.S., and Weiss, A.
1059 (2010). ZAP-70: an essential kinase in T-cell signaling. Cold Spring Harb Perspect Biol *2*, a002279-
1060 a002279.
1061 Wang, Q., Zhang, Y., Wu, L., Niu, S., Song, C., Zhang, Z., Lu, G., Qiao, C., Hu, Y., Yuen, K.-Y.*, et al.* (2020).
1062 Structural and Functional Basis of SARS-CoV-2 Entry by Using Human ACE2. Cell *181*, 894-904.e899.
1063 Weiskopf, D., Schmitz, K.S., Raadsen, M.P., Grifoni, A., Okba, N.M.A., Endeman, H., van den Akker, J.P.C.,
1064 Molenkamp, R., Koopmans, M.P.G., van Gorp, E.C.M.*, et al.* (2020). Phenotype and kinetics of SARS-CoV-
1065 2–specific T cells in COVID-19 patients with acute respiratory distress syndrome. Science Immunology *5*,
1066 eabd2071.
1067 Wilson, J.M. (2004). Adeno-associated virus and lentivirus pseudotypes for lung-directed gene therapy.
1068 Proceedings of the American Thoracic Society *1*, 309-314.
1069 Winkler, E.S., Bailey, A.L., Kafai, N.M., Nair, S., McCune, B.T., Yu, J., Fox, J.M., Chen, R.E., Earnest, J.T.,
1070 Keeler, S.P.*, et al.* (2020). SARS-CoV-2 infection of human ACE2-transgenic mice causes severe lung
1071 inflammation and impaired function. Nature immunology.
1072 Wu, F., Zhao, S., Yu, B., Chen, Y.-M., Wang, W., Song, Z.-G., Hu, Y., Tao, Z.-W., Tian, J.-H., Pei, Y.-Y.*, et al.*
1073 (2020a). A new coronavirus associated with human respiratory disease in China. Nature *579*, 265-269.
1074 Wu, M., Chen, Y., Xia, H., Wang, C., Tan, C.Y., Cai, X., Liu, Y., Ji, F., Xiong, P., Liu, R.*, et al.* (2020b).
1075 Transcriptional and proteomic insights into the host response in fatal COVID-19 cases. Proceedings of
1076 the National Academy of Sciences *117*, 28336.
1077 Xia, H., Cao, Z., Xie, X., Zhang, X., Chen, J.Y.-C., Wang, H., Menachery, V.D., Rajsbaum, R., and Shi, P.-Y.
1078 (2020). Evasion of Type I Interferon by SARS-CoV-2. Cell Reports *33*, 108234.
1079 Yan, K., Vet, L.J., Tang, B., Hobson-Peters, J., Rawle, D.J., Le, T.T., Larcher, T., Hall, R.A., and Suhrbier, A.
1080 (2020). A Yellow Fever Virus 17D Infection and Disease Mouse Model Used to Evaluate a Chimeric
1081 Binjari-Yellow Fever Virus Vaccine. Vaccines *8*.

1082 Yinda, C.K., Port, J.R., Bushmaker, T., Offei Owusu, I., Purushotham, J.N., Avanzato, V.A., Fischer, R.J.,
1083 Schulz, J.E., Holbrook, M.G., Hebner, M.J., *et al.* (2021). K18-hACE2 mice develop respiratory disease
1084 resembling severe COVID-19. PLoS Pathog *17*, e1009195.
1085 Zhao, X., Chen, D., Szabla, R., Zheng, M., Li, G., Du, P., Zheng, S., Li, X., Song, C., Li, R., *et al.* (2020). Broad
1086 and Differential Animal Angiotensin-Converting Enzyme 2 Receptor Usage by SARS-CoV-2. Journal of
1087 virology *94*.
1088 Zhou, P., Yang, X.-L., Wang, X.-G., Hu, B., Zhang, L., Zhang, W., Si, H.-R., Zhu, Y., Li, B., Huang, C.-L., *et al.*
1089 (2020). A pneumonia outbreak associated with a new coronavirus of probable bat origin. Nature *579*,
1090 270-273.
1091 Zhu, Y., Wang, W., and Wang, X. (2015). Roles of transcriptional factor 7 in production of inflammatory
1092 factors for lung diseases. J Transl Med *13*, 273-273.

1093

Figure 1

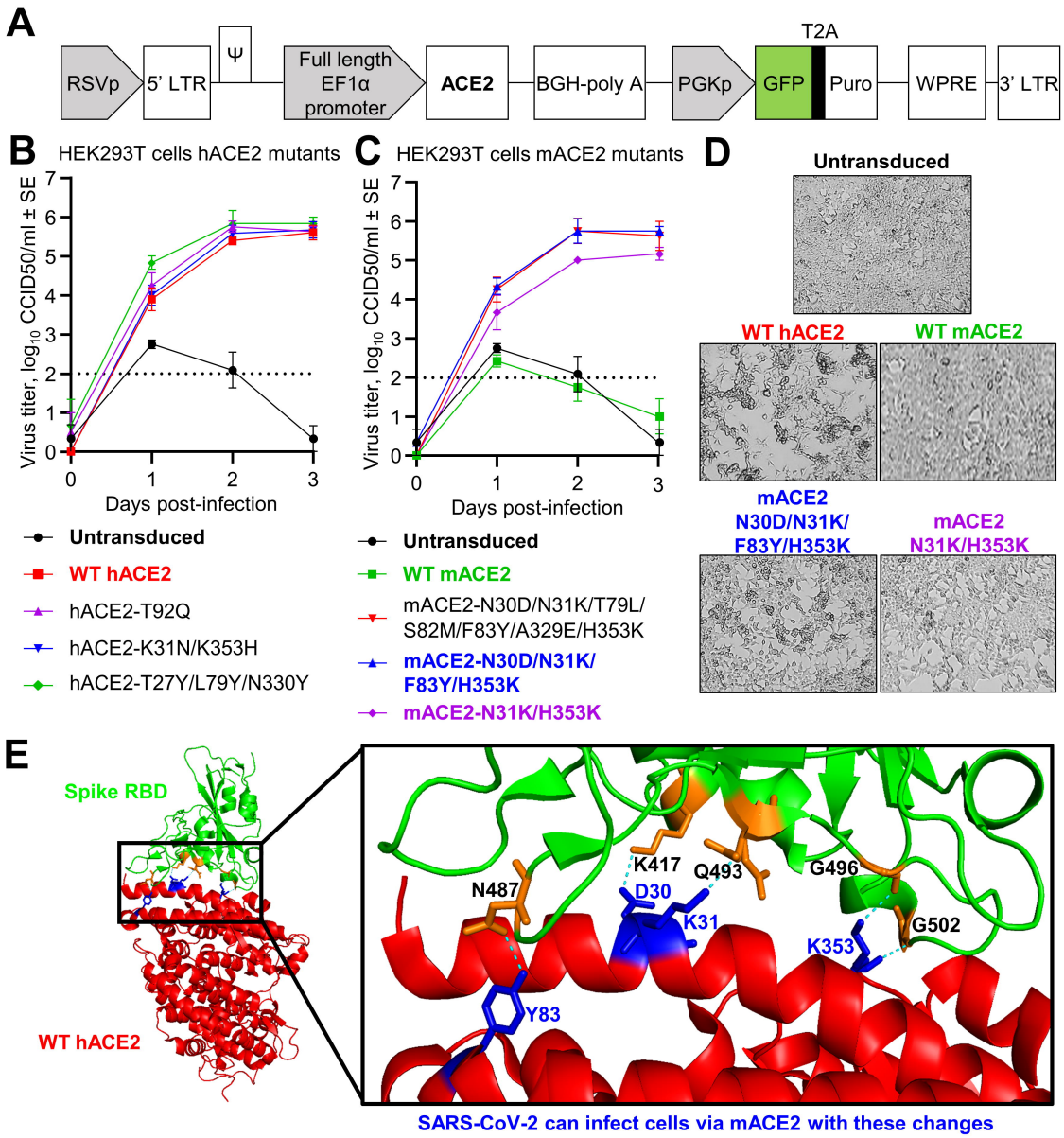
A
RSVp
5' LTR
Ψ
Full length EF1α promoter
ACE2
BGH-poly A
PGKp
T2A
GFP
Puro
WPRE
3' LTR
B
HEK293T cells hACE2 mutants
Virus titer, log10 CCID50/ml ± SE
Days post-infection
Untransduced
WT hACE2
hACE2-T92Q
hACE2-K31N/K353H
hACE2-T27Y/L79Y/N330Y
C
HEK293T cells mACE2 mutants
Virus titer, log10 CCID50/ml ± SE
Days post-infection
Untransduced
WT mACE2
mACE2-N30D/N31K/T79L/S82M/F83Y/A329E/H353K
mACE2-N30D/N31K/F83Y/H353K
mACE2-N31K/H353K
D
Untransduced
WT hACE2
WT mACE2
mACE2 N30D/N31K/F83Y/H353K
mACE2 N31K/H353K
E
Spike RBD
WT hACE2
N487
K417
D30
Q493
G496
K31
G502
K353
Y83
SARS-CoV-2 can infect cells via mACE2 with these changes

Figure 2

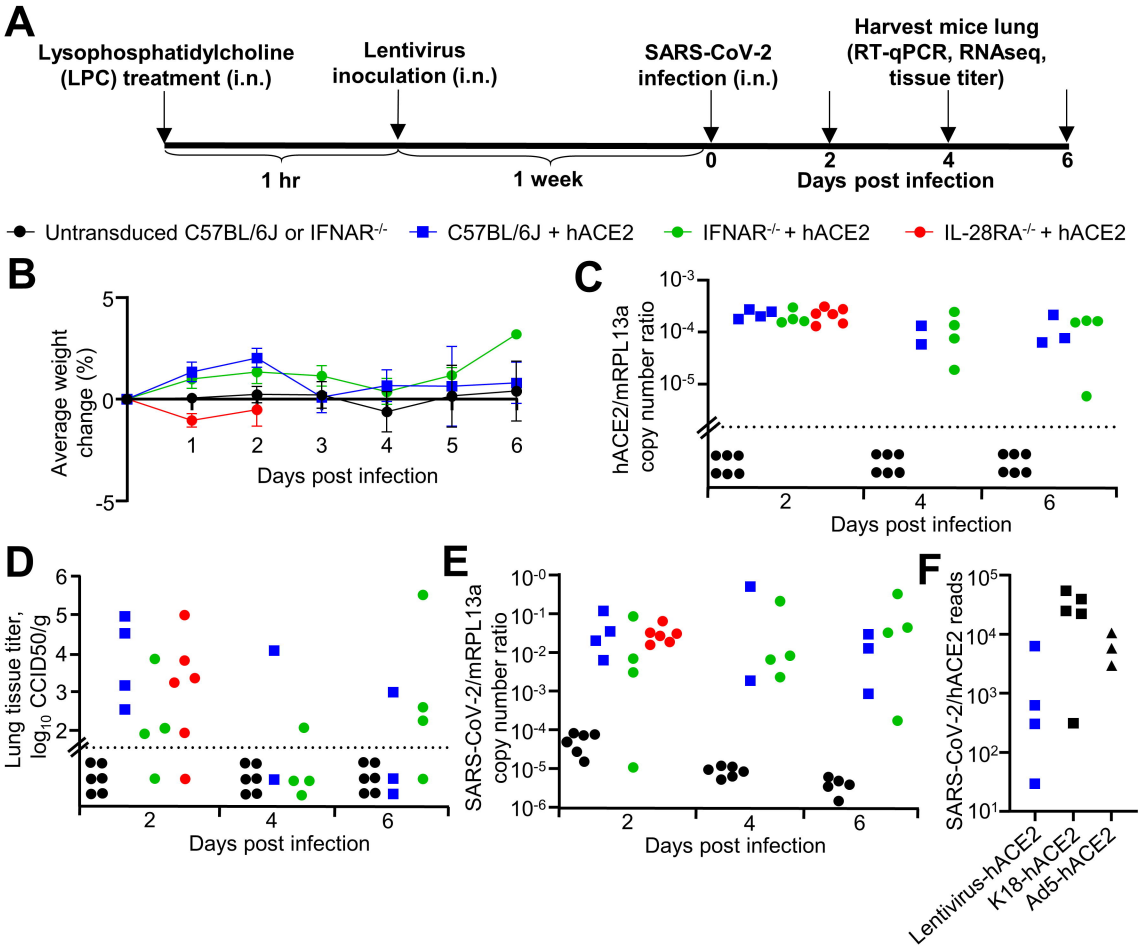
A
Lysophosphatidylcholine (LPC) treatment (i.n.)
Lentivirus inoculation (i.n.)
SARS-CoV-2 infection (i.n.)
Harvest mice lung (RT-qPCR, RNAseq, tissue titer)
1 hr
1 week
0
2
4
6
Days post infection
Untransduced C57BL/6J or IFNAR-/-
C57BL/6J + hACE2
IFNAR-/- + hACE2
IL-28RA-/- + hACE2
B
Average weight change (%)
Days post infection
C
hACE2/mRPL13a copy number ratio
Days post infection
D
Lung tissue titer, log10 CCID50/g
Days post infection
E
SARS-CoV-2/mRPL13a copy number ratio
Days post infection
F
SARS-CoV-2/hACE2 reads
Lentivirus-hACE2
K18-hACE2
Ad5-hACE2

Figure 3

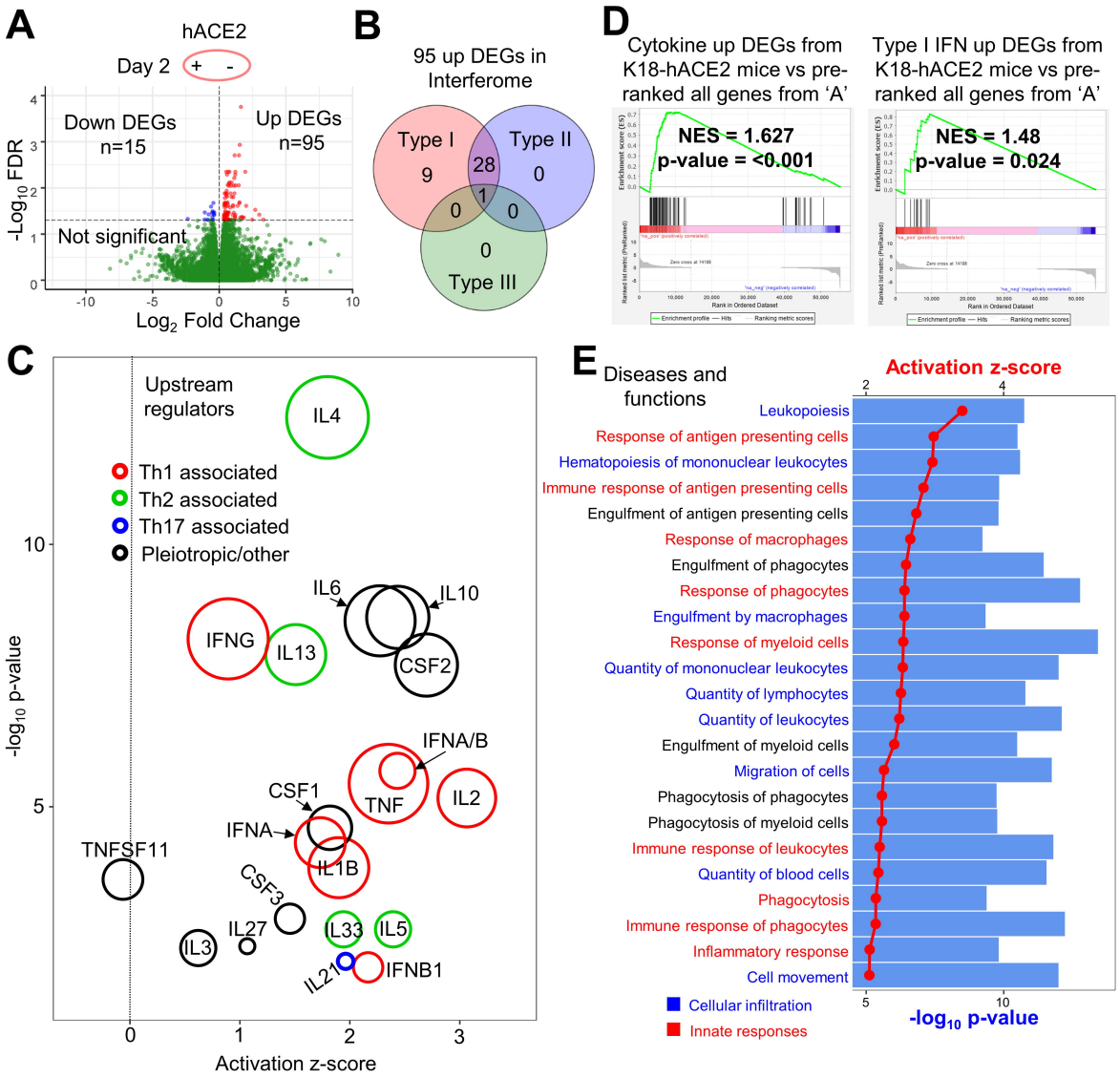

F

Human COVID-19 lung up DEGs vs pre-ranked all genes from 'A'

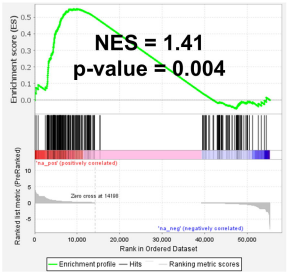

Core enriched genes analysed by GO Biological Processes ontology (Enrichr). Top 10 sorted by p-value:

GO process	P-value
cytokine-mediated signaling pathway	1.39E-20
cellular response to type I interferon	8.70E-20
type I interferon signaling pathway	8.70E-20
cellular response to interferon-gamma	4.33E-13
chemokine-mediated signaling pathway	6.10E-09
response to interferon-gamma	4.14E-08
inflammatory response	4.36E-08
lymphocyte chemotaxis	7.20E-08
eosinophil migration	1.01E-07
eosinophil chemotaxis	1.01E-07

Figure 4

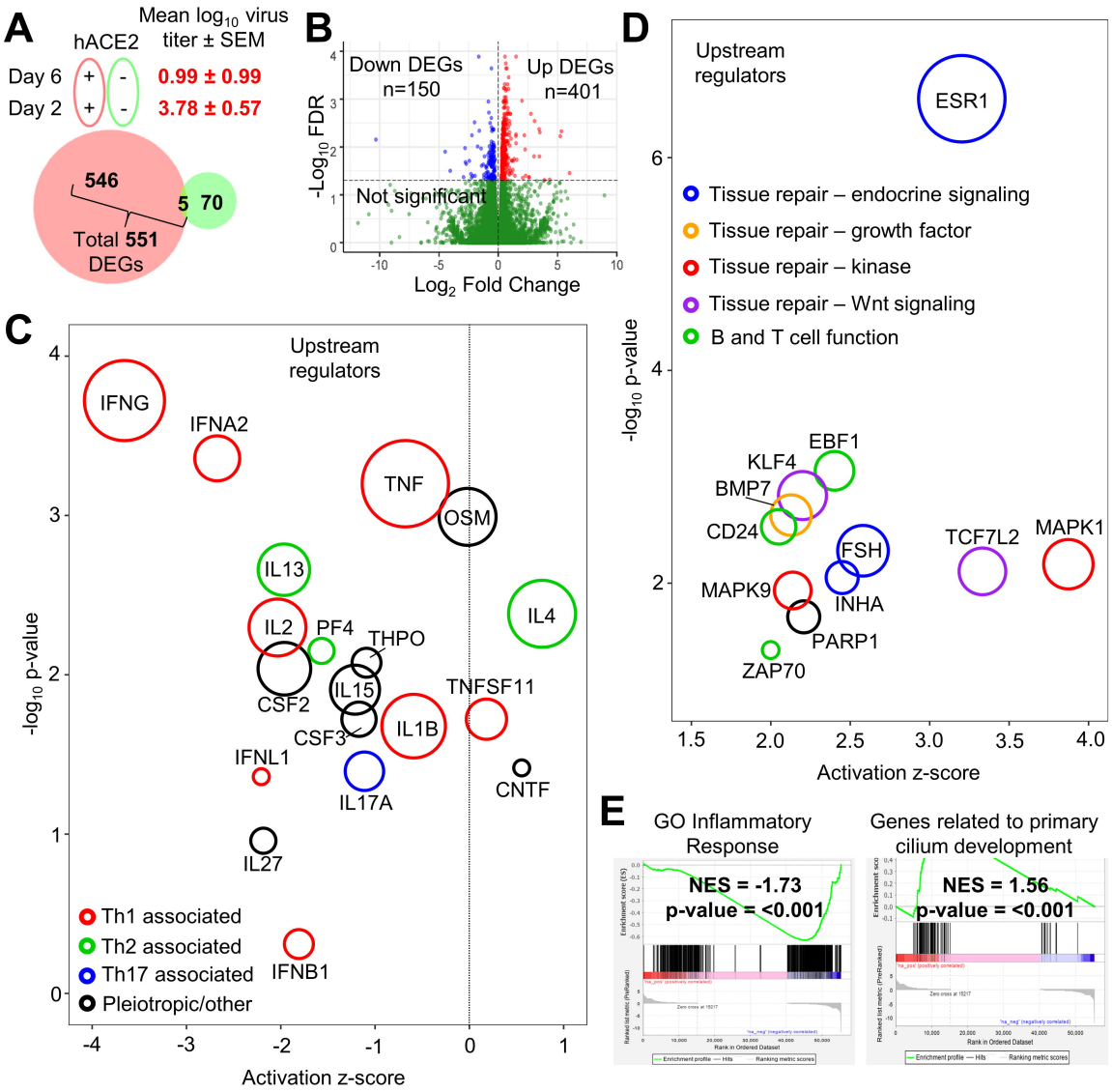
A
hACE2
Mean log10 virus titer ± SEM
Day 6 + - 0.99 ± 0.99
Day 2 + - 3.78 ± 0.57
546
5 70
Total 551 DEGs
B
Down DEGs n=150
Up DEGs n=401
Not significant
-Log10 FDR
Log2 Fold Change
C
Upstream regulators
IFNG
IFNA2
TNF
OSM
IL13
IL4
IL2
PF4
THPO
CSF2
IL15
TNFSF11
CSF3
IL1B
IFNL1
IL17A
CNTF
IL27
IFNB1
Th1 associated
Th2 associated
Th17 associated
Pleiotropic/other
-log10 p-value
Activation z-score
D
Upstream regulators
ESR1
Tissue repair – endocrine signaling
Tissue repair – growth factor
Tissue repair – kinase
Tissue repair – Wnt signaling
B and T cell function
EBF1
KLF4
BMP7
CD24
FSH
TCF7L2
MAPK1
MAPK9
INHA
PARP1
ZAP70
-log10 p-value
Activation z-score
E
GO Inflammatory Response
NES = -1.73
p-value = <0.001
Genes related to primary cilium development
NES = 1.56
p-value = <0.001

Figure 5

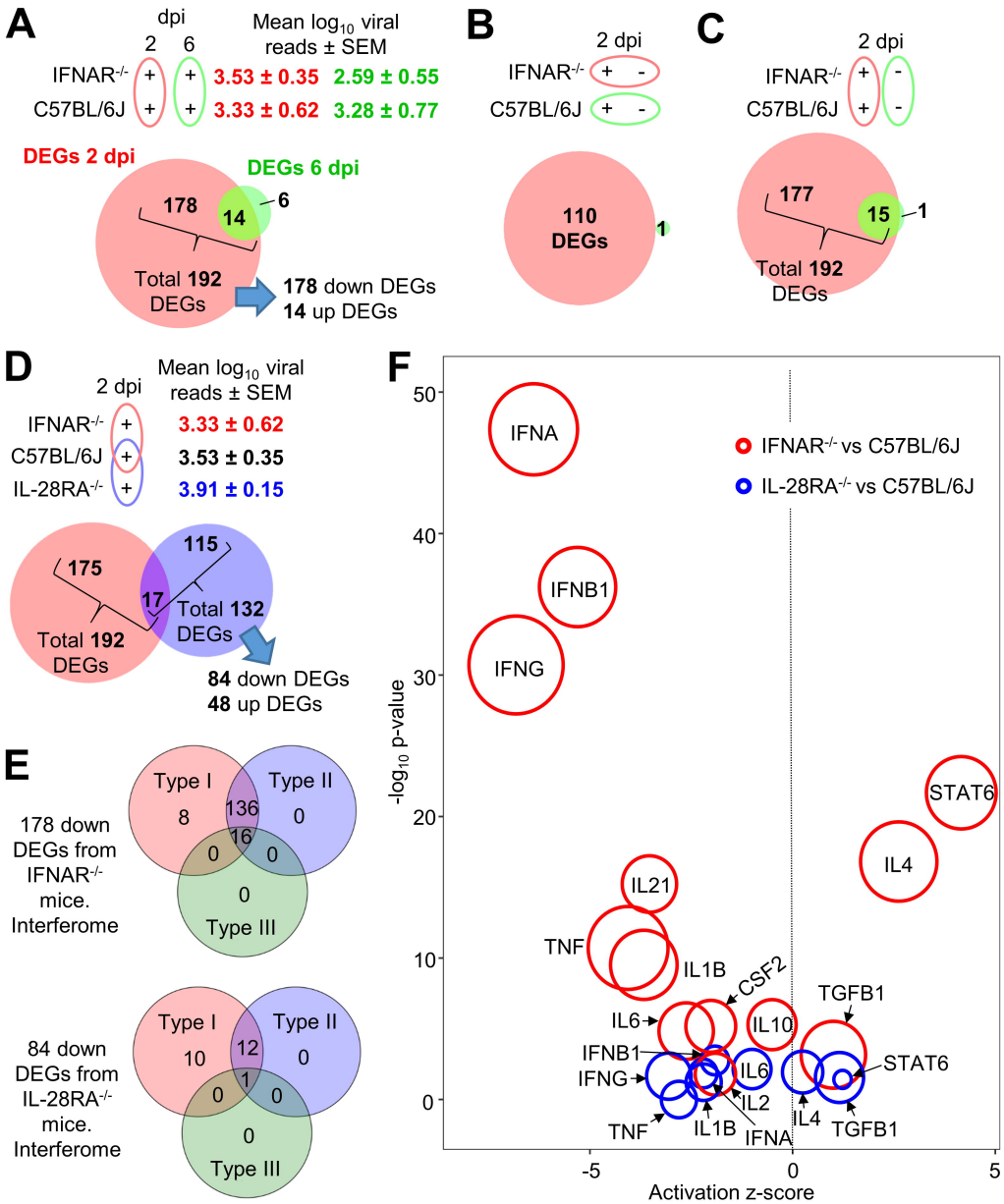
A
dpi
2 6
Mean log10 viral reads ± SEM
IFNAR-/- + + 3.53 ± 0.35 2.59 ± 0.55
C57BL/6J + + 3.33 ± 0.62 3.28 ± 0.77
DEGs 2 dpi
DEGs 6 dpi
178
14
6
Total 192 DEGs
178 down DEGs
14 up DEGs
B
2 dpi
IFNAR-/- + -
C57BL/6J + -
110 DEGs
1
C
2 dpi
IFNAR-/- + -
C57BL/6J + -
177
15
1
Total 192 DEGs
D
2 dpi
Mean log10 viral reads ± SEM
IFNAR-/- + 3.33 ± 0.62
C57BL/6J + 3.53 ± 0.35
IL-28RA-/- + 3.91 ± 0.15
175
115
17
Total 192 DEGs
Total 132 DEGs
84 down DEGs
48 up DEGs
E
178 down DEGs from IFNAR-/- mice. Interferome
Type I
Type II
Type III
8
136
0
16
0
0
0
84 down DEGs from IL-28RA-/- mice. Interferome
Type I
Type II
Type III
10
12
0
1
0
0
0
F
IFNAR-/- vs C57BL/6J
IL-28RA-/- vs C57BL/6J
-log10 p-value
Activation z-score
IFNA
IFNB1
IFNG
STAT6
IL4
IL21
TNF
IL1B
CSF2
TGFB1
IL6
IL10
IFNB1
IFNG
IL6
IL2
STAT6
TNF
IL1B
IFNA
IL4
TGFB1

Figure 6

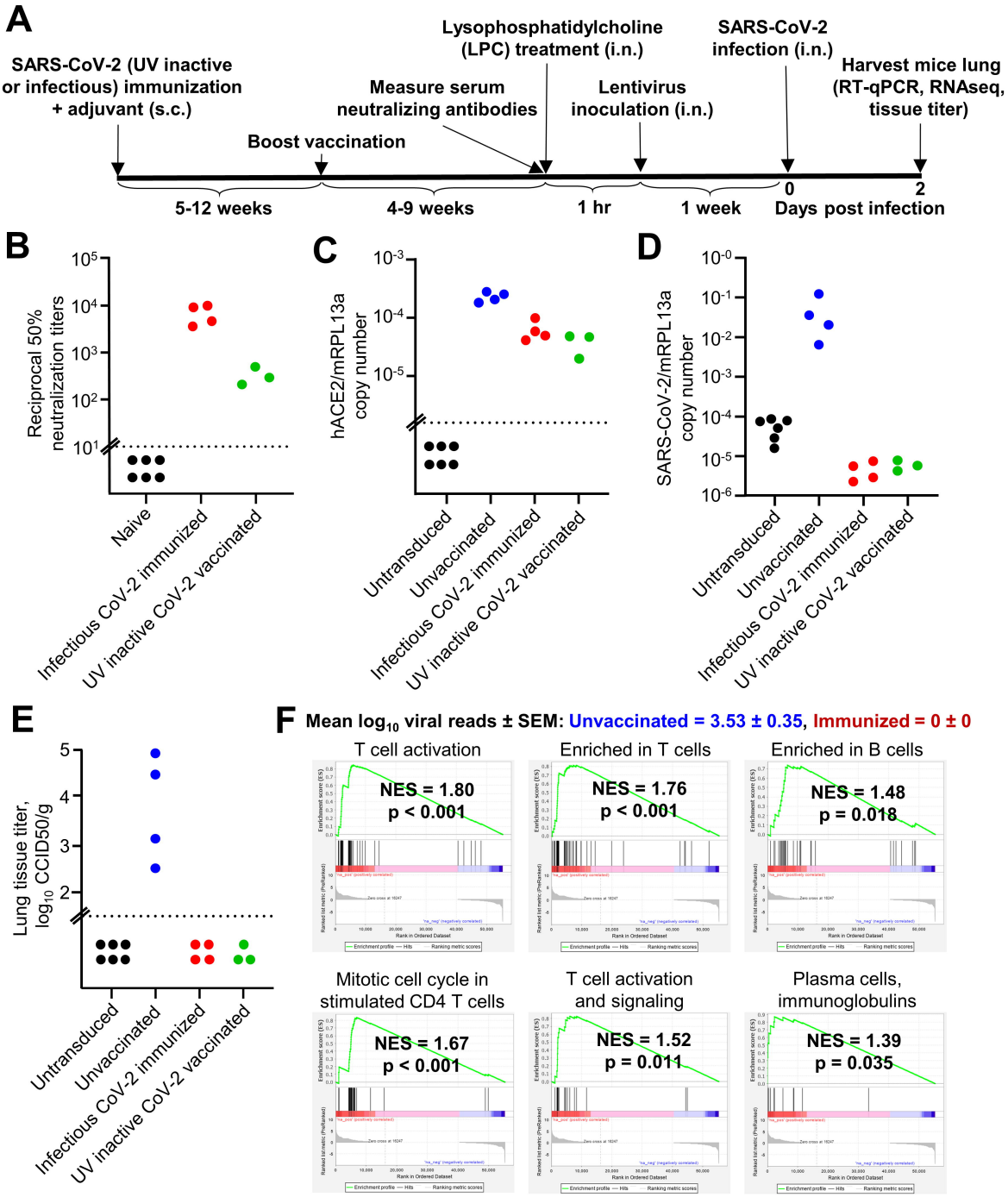
A
SARS-CoV-2 (UV inactive or infectious) immunization + adjuvant (s.c.)
Boost vaccination
Measure serum neutralizing antibodies
Lysophosphatidylcholine (LPC) treatment (i.n.)
Lentivirus inoculation (i.n.)
SARS-CoV-2 infection (i.n.)
Harvest mice lung (RT-qPCR, RNAseq, tissue titer)
5-12 weeks
4-9 weeks
1 hr
1 week
0
2
Days post infection
B
Reciprocal 50% neutralization titers
Naive
Infectious CoV-2 immunized
UV inactive CoV-2 vaccinated
C
hACE2/mRPL13a copy number
Untransduced
Unvaccinated
Infectious CoV-2 immunized
UV inactive CoV-2 vaccinated
D
SARS-CoV-2/mRPL13a copy number
Untransduced
Unvaccinated
Infectious CoV-2 immunized
UV inactive CoV-2 vaccinated
E
Lung tissue titer, log10 CCID50/g
Untransduced
Unvaccinated
Infectious CoV-2 immunized
UV inactive CoV-2 vaccinated
F Mean log10 viral reads ± SEM: Unvaccinated = 3.53 ± 0.35, Immunized = 0 ± 0
T cell activation
NES = 1.80
p < 0.001
Enriched in T cells
NES = 1.76
p < 0.001
Enriched in B cells
NES = 1.48
p = 0.018
Mitotic cell cycle in stimulated CD4 T cells
NES = 1.67
p < 0.001
T cell activation and signaling
NES = 1.52
p = 0.011
Plasma cells, immunoglobulins
NES = 1.39
p = 0.035

Supplementary figure 1

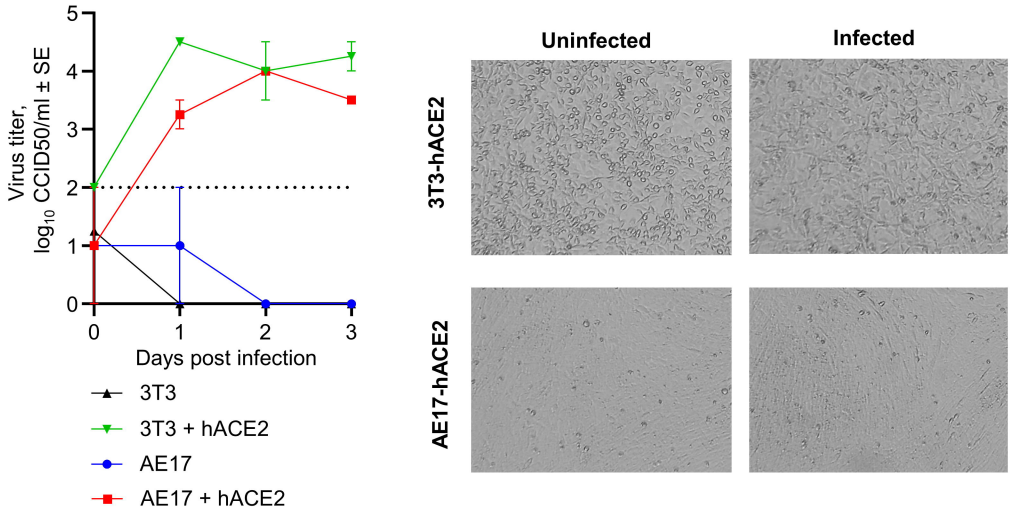

Supplementary figure 2

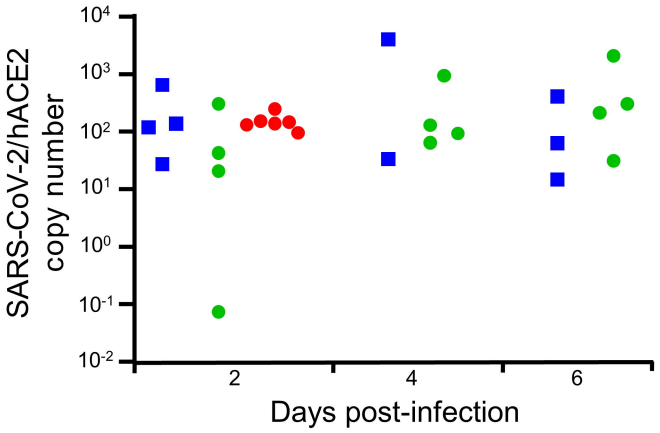
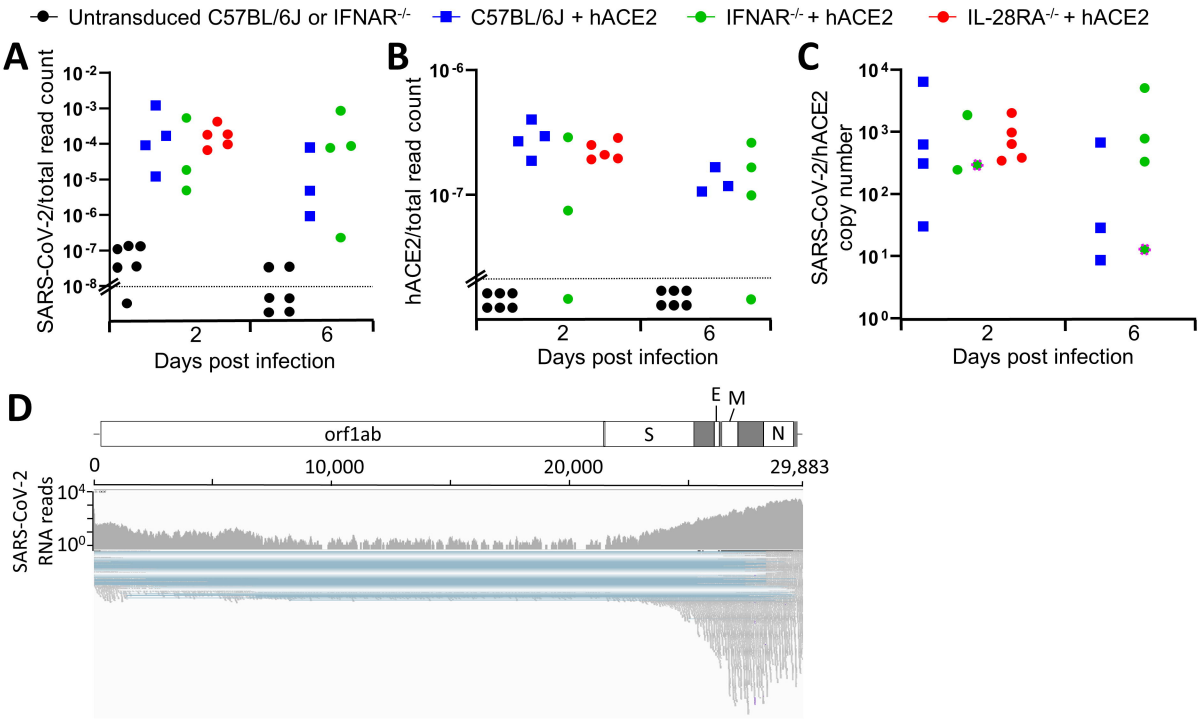
Supplementary figure 3